



A coupled model for the dynamics of gas exchanges in the human lung with Haldane and Bohr's effects

Laurent Boudin, Céline Grandmont, Bérénice Grec, Sébastien Martin

► To cite this version:

Laurent Boudin, Céline Grandmont, Bérénice Grec, Sébastien Martin. A coupled model for the dynamics of gas exchanges in the human lung with Haldane and Bohr's effects. *Journal of Theoretical Biology*, In press, pp.111590. 10.1016/j.jtbi.2023.111590 . hal-03883301v2

HAL Id: hal-03883301

<https://hal.science/hal-03883301v2>

Submitted on 1 Sep 2023

HAL is a multi-disciplinary open access archive for the deposit and dissemination of scientific research documents, whether they are published or not. The documents may come from teaching and research institutions in France or abroad, or from public or private research centers.

L'archive ouverte pluridisciplinaire **HAL**, est destinée au dépôt et à la diffusion de documents scientifiques de niveau recherche, publiés ou non, émanant des établissements d'enseignement et de recherche français ou étrangers, des laboratoires publics ou privés.

A COUPLED MODEL FOR THE DYNAMICS OF GAS EXCHANGES IN THE HUMAN LUNG WITH HALDANE AND BOHR'S EFFECTS

LAURENT BOUDIN, CÉLINE GRANDMONT, BÉRÉNICE GREC, AND SÉBASTIEN MARTIN

ABSTRACT. We propose an integrated dynamical model for oxygen and carbon dioxide transfer from the lung into the blood, coupled with a lumped mechanical model for the ventilation process, for healthy patients as well as in pathological cases. In particular, we take into account the nonlinear interaction between oxygen and carbon dioxide in the blood volume, referred to as the Bohr and Haldane effects. We also propose a definition of the physiological dead space volume (the lung volume that does not contribute to gas exchange) which depends on the pathological state and the breathing scenario. This coupled ventilation-gas diffusion model is driven by the sole action of the respiratory muscles. We analyse its sensitivity with respect to characteristic parameters: the resistance of the bronchial tree, the elastance of the lung tissue and the oxygen and carbon dioxide diffusion coefficients of the alveolo-capillary membrane. Idealized pathological situations are also numerically investigated. We obtain realistic qualitative tendencies, which represent a first step towards classification of the pathological behaviours with respect to the considered input parameters.

CONTENTS

1. Introduction	2
2. A 0D model for the respiratory system	3
2.1. Mechanical model	3
2.2. Gas exchange model	4
2.3. Computation of the alveolo-capillary fluxes	6
2.4. Summary of the 0D model	9
3. Gas exchange model for oxygen and carbon dioxide	10
3.1. Balance of oxygen including the Bohr effect	10
3.2. Balance of carbon dioxide including the Haldane effect	12
3.3. Quantitative study of the coupled diffusion process	13
4. Healthy reference respiration scenarios	16
4.1. Normal breathing	16
4.2. Hyperventilation	18
5. Parameter sensitivity	19
5.1. Global structuration	19
5.2. Crossed sensitivity structuring	21
6. Characteristic cases, tendencies	24
6.1. Happy hypoxia	24
6.2. Asthma	24
6.3. Pathologies affecting tissue elasticity	26
7. Conclusion	28
Appendix A. Parameters	28
References	28
Declaration of interests	30

1. INTRODUCTION

The main function of the respiratory system is to ensure the oxygen transfer from the outside air to the blood and the carbon dioxide transfer from the blood to the outside air. Those transfers are achieved thanks to passive diffusion through the alveolo-capillary membrane which separates two phases: the alveolar air on the one side, the blood on the other side. The gas exchanges at this level require air renewal, which happens during the mechanical ventilation process.

The ventilation process involves the air transport through the resistive bronchial tree, which irrigates the elastic lung tissue called parenchyma. Driven by the diaphragm contraction, the parenchyma is deformed, inducing a pressure drop between the alveoli and the mouth, and consequently an airflow. There is a hierarchy of models which can describe this phenomenon. Models involving ordinary differential equations, possibly nonlinear and complex, may be considered, as in [27, 30, 13, 19], using for example nonlinear double-balloon models. The air transport can further be described with unsteady one-dimensional advection-diffusion partial differential equations, see [19, 22, 23] for instance, and even with either unsteady systems describing the three-dimensional air flow, e.g. [2, 24], or a resistive tree interacting with a three-dimensional elasticity model as in [26, 6, 25].

In this paper, we choose to consider a simple mechanical model for the ventilation process. It is similar to the ones from [3, 5, 4, 34]: a single-compartment model, often represented under the form of a balloon corresponding to the lungs, connected to a pipe representing the airways. There are mainly two physiological parameters involved in this model. The lung elastance E measures the stiffness related to the stretching forces, so that the lung spontaneously comes back to rest. The pulmonary resistance R measures the resistive forces in the whole bronchial tree (due to the friction between the gas molecules and the airway walls) and the resistive forces to deformation inside tissues (due to the friction between the lung tissues and the chest wall). Those critical parameters are affected in pathological situations, which can induce substantial modifications of the elastance (fibrosis, emphysema...), of the resistance (asthma, COPD...), but also of other physiological parameters.

The lung mechanical function is to serve as a pump for the air renewing to bring oxygen inside the lung and expel the carbon dioxide produced within the body. Thus we need to describe the dynamics of each species concentrations at the alveolar level. The gaseous exchange involves a passive diffusion process through the alveolo-capillary membrane together with the binding of oxygen and carbon dioxide to hemoglobin. The diffusion process of both gases through the alveolo-capillary membrane is characterized by two constant diffusion coefficients, denoted by D_{m,O_2} and D_{m,CO_2} , and is driven by the blood-alveolar partial pressure drops of each species. The affinity of hemoglobin with respect to oxygen depends on the blood pressure of carbon dioxide, which is referred to as the Haldane and Bohr effects in the literature, see [11, 28, 9, 10, 18]. Those effects induce a nonlinear coupling in the dynamics of the diffusion process of each species. Roughly speaking, Haldane's effect is due to the fact that the blood oxygen increases the carbon dioxide removal, and Bohr's refers to the shift of oxygen-binding affinity with respect to both pH and carbon dioxide concentration. Consequently, the nonlinear coupled dynamics of the blood partial pressures of oxygen and carbon dioxide, based upon a mole balance, may lead to substantial modifications on the gas transfer in pathological situations. For instance, in emphysema, diffusion permeabilities are lowered, leading to possible kinetic limitation in the instantaneous gas transfer.

The gas exchanges may be widely affected by the so-called lung dead space, *i.e.* the volume of air not involved in the gas exchanges, see, for instance, [10, 34]. This dead space is here chosen as the sum of the anatomic dead space and an extra volume depending on the patient state and on the breathing scenario. In particular, the air entering the alveoli during inspiration is a mixture of dead-space air, assumed to be filled of gases whose mole fractions are the current ones in the lung, and fresh air. Higher values of the dead space may have a strong impact on the air renewing and

thus the gas transfer. Hence, it is crucial to properly model the dead space, and more precisely, in our model, the extra volume, which we call here the pathological dead space: it is close to zero when the patient is healthy, but can become significantly non-zero for asthmatic or emphysematous patients, for example.

Note that very complex ODE systems modelling the whole respiratory process have also been proposed in the literature, as in [8]. Such systems also include cardiovascular phenomena and central neural control. In this work, we aim to focus only on the ventilation-diffusion coupling with a limited number of physiological parameters, which can moreover be calibrated and physically interpreted.

The paper is hence organised as follows. In Section 2, we present our ventilation-diffusion model, which can capture the main observable quantities for a healthy patient at rest. In Section 3, we further discuss the gas exchanges and provide a relevant model for both Bohr and Haldane effects. We then start the numerical studies by first investigating some reference situations for a healthy patient in Section 4, which allows to check the relevant behaviour of our model. Next, in Section 5, we lead a sensitivity analysis with respect to the parameters R , E and D_m to study their influence on the gas transfer efficiency, in order to find possible global structuring or crossed effects with respect to those parameters. Eventually, Section 6 is dedicated to exploring the behaviour of our model in various pathological situations.

2. A 0D MODEL FOR THE RESPIRATORY SYSTEM

In this section, we present the ventilation-perfusion dynamical model for oxygen and carbon dioxide. The first step is the description of the standard mechanical ventilation model, for which we define the associated pathological dead space. Further, we discuss the gas-exchange process, based upon mole balances for both species. Last, we focus on the computation of the gaseous fluxes at the alveolo-capillary level.

2.1. Mechanical model. Let us first write the simple linear lung mechanical model we use here. As we already emphasized, it involves two main ingredients: the resistance R of the branches connecting alveoli to the outside air, and the elastic properties of the surrounding medium measured by the elastance E . Denoting by $T_{\text{fin}} > 0$ the experiment final time, the time-depending lung volume V and its time derivative \dot{V} , which is the corresponding air flow, satisfy, for any $t \in [0, T_{\text{fin}}]$,

$$(1) \quad R \dot{V}(t) + E(V(t) - \text{FRC}) = -P_{\text{ext}}(t),$$

supplemented with an initial condition on V . In (1), FRC is the functional residual volume (volume at rest) for a healthy patient, $P_{\text{ext}}(t)$ is the muscular pressure leading to the deformation of the lung parenchyma, which induces inspiration (and possibly forced expiration) at time t . This last quantity, often referred to as the airway opening or trans-pulmonary pressure [27, 5], is chosen here as a periodic function, and we denote by $T \in (0, T_{\text{fin}}]$ the corresponding period. Unfortunately, the pressure is not accessible to direct measurements. It accounts for the effort of the diaphragm ($P_{\text{ext}}(t) < 0$ for inspiration), and possibly of the abdomen muscles during a forced expiration ($P_{\text{ext}}(t) = 0$ for passive expiration and $P_{\text{ext}}(t) > 0$ for forced expiration). Note that, for the sake of simplicity, in all the upcoming computations, $t = 0$ corresponds to the beginning of a respiratory cycle, and we set $V(0) = \text{FRC}$. The final time T_{fin} will be chosen as a multiple of T in order to deal with full respiratory cycles.

For the air renewing process, we need to describe the dynamics of both oxygen and carbon dioxide at the alveolar level. This dynamics takes place in the volume of air available in the lung for gas exchanges. From the modelling point of view, the total volume V can be split into two contributions: the so-called lung dead space, denoted by V_D , which does not contribute to gas exchanges, and $V - V_D$ which is involved in the exchanges. The dead volume is assumed to be constant during each respiratory cycle, as the sum of the anatomic dead space V_D^A and the extra

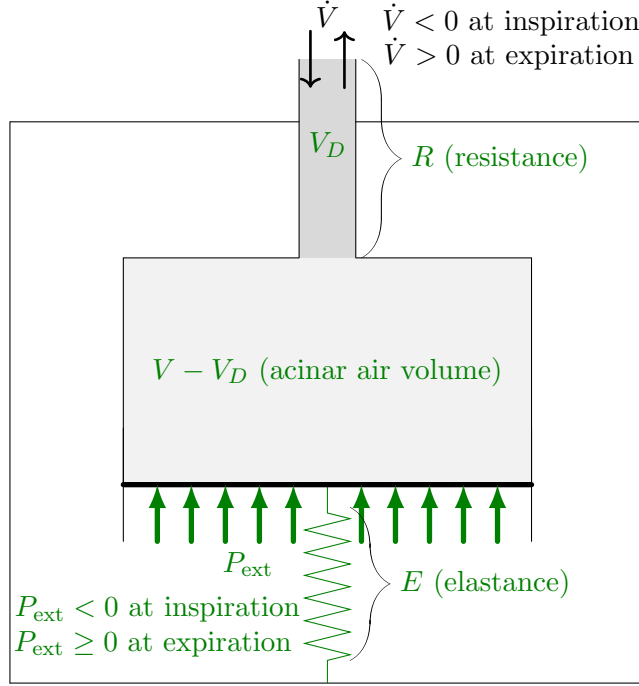


FIGURE 1. Schematic view of the lung mechanics.

volume V_D^P depending on the patient state:

$$(2) \quad V_D = V_D^A + V_D^P.$$

The usual value of V_D^A is 0.15 L [34]. We choose to define the extra pathological dead space for each respiratory cycle $[kT, (k+1)T]$, $k \geq 0$, as

$$(3) \quad V_D^P = \max(V(kT) - \text{FRC}, 0).$$

This volume measures the discrepancy between a non-pathological functional residual volume FRC and the computed volume at the end of each expiration. The computation is performed according to the mechanical dynamics of the ventilation and thus depends on the patient characteristics R , E and the breathing scenario P_{ext} , see Remark 1. Note that it is adapted to the patient breathing at each respiratory cycle. The quantity V_D^P is nonnegative, and close to 0 in healthy situations.

The lung mechanics is schematically described in Figure 1.

Remark 1. *Note that, when the applied external pressure is periodic, there exists a unique periodic solution to (1). This solution is moreover asymptotically stable [20]. It implies that, in the periodic regime limit, V_D^P (and thus ϕ) takes the very same value $V_{D_{\text{per}}}^P$ at each respiratory cycle, which can be exactly computed as*

$$V_{D_{\text{per}}}^P = \max\left(-\frac{1}{R(1 - e^{-T/\tau})} \int_0^T e^{-(T-s)/\tau} P_{\text{ext}}(s) ds, 0\right).$$

It depends on the parameters of the mechanical model, and in particular on the relaxation time $\tau = R/E$, as well as on the applied external pressure. For instance, it cannot be neglected when the lung resistance R increases or its elastance E decreases.

2.2. Gas exchange model. The gas dynamics description requires the introduction of the mole fractions of oxygen χ_{O_2} and carbon dioxide χ_{CO_2} in the alveoli, so that the volume of oxygen, respectively carbon dioxide, in the available space is $\chi_{\text{O}_2}(V - V_D)$, respectively $\chi_{\text{CO}_2}(V - V_D)$.

The variations of gas quantities in the alveolar space are due to fluxes of only two types, see Figure 2: the fluxes at the entrance of the acini, denoted by $q_{O_2}^{\text{up}}$ for oxygen and $q_{CO_2}^{\text{up}}$ for carbon dioxide, and the fluxes at the alveolo-capillary membrane, denoted by q_{O_2} for oxygen and q_{CO_2} for carbon dioxide.

Let us describe the mole balances for oxygen and carbon dioxide in the alveolar space. At the acini entrance, we have to discuss the difference between inspiration and expiration. During inspiration ($\dot{V} > 0$), the flux of oxygen entering the alveoli is $\chi_{O_2}^0 \dot{V} > 0$, where $\chi_{O_2}^0$ is the oxygen mole fraction of the air entering the alveoli. During expiration ($\dot{V} < 0$), the flux is $\chi_{O_2} \dot{V} < 0$, as oxygen is exhaled from the acinar space. Thus we have

$$q_{O_2}^{\text{up}} = \mathbb{1}_{\mathbb{R}_+}(\dot{V})\chi_{O_2}^0 \dot{V} + \mathbb{1}_{\mathbb{R}_-}(\dot{V})\chi_{O_2} \dot{V},$$

where we denote by $\mathbb{1}_{\mathbb{R}_\pm}(z)$ the quantity equal to 1 if $z \in \mathbb{R}_\pm$ and 0 otherwise. Using the same argument with carbon dioxide, we can write

$$q_{CO_2}^{\text{up}} = \mathbb{1}_{\mathbb{R}_+}(\dot{V})\chi_{CO_2}^0 \dot{V} + \mathbb{1}_{\mathbb{R}_-}(\dot{V})\chi_{CO_2} \dot{V}.$$

At the alveolo-capillary membrane, the flux q_{O_2} of oxygen diffusing from the alveoli onto the blood is usually positive. For carbon dioxide, the net flux from the alveoli to the blood, denoted by q_{CO_2} , is negative (as carbon dioxide is removed from the blood to the acinus in order to be exhaled). So far, q_{O_2} and q_{CO_2} need to be precisely defined, which is the subject of subsection 2.3. These quantities are crucial from the functional point of view, since the mean fluxes are related to the amount of energy provided to the body (oxygen flux) and the amount of waste product which is exhaled from the body (carbon dioxide flux).

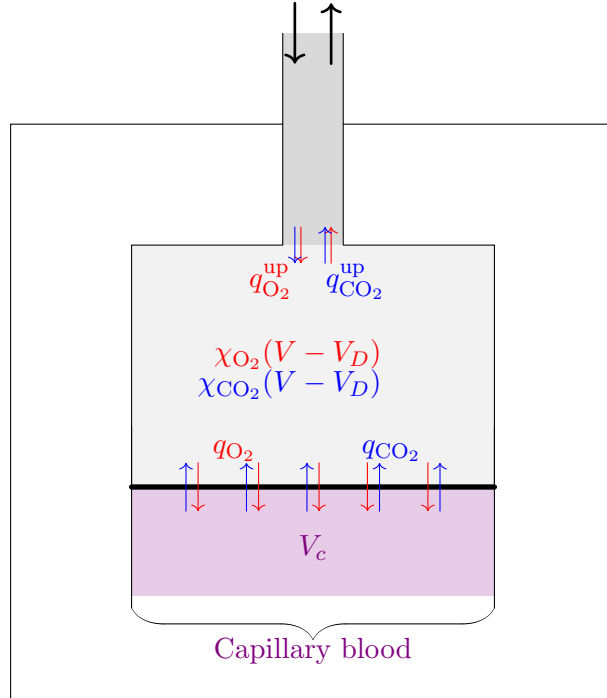


FIGURE 2. Schematic view of the gas exchange model.

The evolution of the oxygen volume in the alveolar space can thus be expressed as

$$\frac{d}{dt} (\chi_{O_2}(V - V_D)) = q_{O_2}^{\text{up}} - q_{O_2}.$$

Then using that V_D does not depend on time during each respiratory cycle, we obtain

$$(4) \quad \dot{\chi}_{O_2}(t) = \frac{1}{V(t) - V_D} \left(\dot{V}(t) (\chi_{O_2}^0(t) - \chi_{O_2}(t)) \mathbb{1}_{\mathbb{R}_+}(\dot{V}(t)) - q_{O_2}(t) \right).$$

The similar process is applied to carbon dioxide, which provides

$$(5) \quad \dot{\chi}_{CO_2}(t) = \frac{1}{V(t) - V_D} \left(\dot{V}(t) (\chi_{CO_2}^0(t) - \chi_{CO_2}(t)) \mathbb{1}_{\mathbb{R}_+}(\dot{V}(t)) - q_{CO_2}(t) \right).$$

Equations (4)–(5) allow to compute the mole fractions of both species in the alveoli at each respiratory cycle, for any $t \in [kT, (k+1)T]$, $k \geq 0$. Let us define the mole fractions $\chi_{O_2}^0(t)$ and $\chi_{CO_2}^0(t)$, which describe the composition of the air entering the alveoli during inspiration. It is a mixture of dead-space air, assumed to be filled of gases whose mole fractions are the current ones in the lung, and fresh air, for which $\chi_{O_2}^{\text{atm}} = 21\%$ and $\chi_{CO_2}^{\text{atm}} = 0.04\%$. The inspired fresh air volume is given by $V(t) - V(kT)$. We can thus write, for any $t \in [kT, (k+1)T]$,

$$(6) \quad \chi_{O_2}^0(t) = (1 - \phi(t))\chi_{O_2}^{\text{atm}} + \phi(t)\chi_{O_2}(t), \quad \chi_{CO_2}^0(t) = (1 - \phi(t))\chi_{CO_2}^{\text{atm}} + \phi(t)\chi_{CO_2}(t),$$

where we set

$$(7) \quad \phi(t) = V_D / (V(t) - V(kT) + V_D) > 0.$$

Using (6), (4)–(5) then become

$$(8) \quad \dot{\chi}_{O_2}(t) = \frac{1}{V(t) - V_D} \left((1 - \phi(t)) \dot{V}(t) (\chi_{O_2}^{\text{atm}} - \chi_{O_2}(t)) \mathbb{1}_{\mathbb{R}_+}(\dot{V}(t)) - q_{O_2}(t) \right),$$

$$(9) \quad \dot{\chi}_{CO_2}(t) = \frac{1}{V(t) - V_D} \left((1 - \phi(t)) \dot{V}(t) (\chi_{CO_2}^{\text{atm}} - \chi_{CO_2}(t)) \mathbb{1}_{\mathbb{R}_+}(\dot{V}(t)) - q_{CO_2}(t) \right).$$

We emphasize that, in order for (6) to make sense, the quantity $(1 - \phi(t))$ must remain nonnegative when $\dot{V}(t) \geq 0$ only, and that is the case: during inspiration, V grows and consequently, $V(t) \geq V(kT)$. Besides, note that (8)–(9) differ from their oxygen-only counterpart in [19] since we take the dead space into account: choosing $V_D = 0$ in (8) allows to recover the corresponding equation from [19]. Nevertheless, even for healthy patients, for whom V_D^P is close to zero, taking into account the anatomic dead space, when considering both gases, is crucial to obtain the right order of magnitude of the carbon dioxide quantities, whereas it is not so crucial when considering oxygen alone, as in [19].

We now need to properly define the diffusive fluxes q_{O_2} and q_{CO_2} .

2.3. Computation of the alveolo-capillary fluxes. We assume that the diffusive properties of the blood-gas barrier are constant and uniform along the capillaries. The diffusion process of both gases through the alveolar membrane is a passive diffusion which is thus characterized by two constant diffusion coefficients denoted by D_{m,O_2} and D_{m,CO_2} . It is moreover driven by the difference between the oxygen (respectively carbon dioxide) alveolar pressure $\chi_{O_2}P_{\text{atm}}$ (respectively $\chi_{CO_2}P_{\text{atm}}$) and the blood gaseous partial pressure which is denoted by P_{O_2} (respectively P_{CO_2}), where P_{atm} stands for the atmospheric pressure. Recall that the carbon dioxide diffusive capacity is twenty times higher than the oxygen one (see [10, Chapter 39, pp. 493 & 499] for instance).

Next we have to describe the dynamics of binding with hemoglobin. The chemical reaction of each species with hemoglobin is assumed to be instantaneous [10, Chapter 39, p. 499]. As already mentioned, there exists a nonlinear coupling between both gases. The interaction of the exchange dynamics of oxygen and carbon dioxide induces what is referred to as the Bohr and Haldane effects. In the Haldane effect, the blood oxygenation displaces carbon dioxide from hemoglobin, which increases the removal of carbon dioxide. Consequently, oxygenated blood has a reduced affinity for carbon dioxide and the Haldane effect describes the ability of hemoglobin to carry increased amounts of carbon dioxide in the deoxygenated state as opposed to the oxygenated state. In the Bohr

effect, oxygen-binding affinity of hemoglobin is inversely related to both acidity and carbon dioxide concentration. It thus refers to the shift, caused by changes in the carbon dioxide concentration or the environment pH, in the oxygen dissociation curve describing the saturation of hemoglobin with respect to the oxygen partial pressure.

Consequently, the dynamic of the blood partial pressures of oxygen and carbon dioxide can be described through functions representing the concentrations $\mathcal{C}_{\text{O}_2} = \mathcal{C}_{\text{O}_2}(P_{\text{O}_2}, P_{\text{CO}_2})$ and $\mathcal{C}_{\text{CO}_2} = \mathcal{C}_{\text{CO}_2}(P_{\text{O}_2}, P_{\text{CO}_2})$ of O_2 and CO_2 in the blood, which are assumed to be uniform at any time in the whole pulmonary capillary blood volume V_c . The expressions of functions \mathcal{C}_{O_2} and $\mathcal{C}_{\text{CO}_2}$ result from the Bohr and Haldane effects modelling the coupling between the gas dynamics and are provided and discussed in subsections 3.1–3.2, see (21) and (24).

Let us now describe the transfer dynamics, as in [31], involves a volume V_c of capillary blood, which is instantaneously brought in the neighbourhood of the alveoli, then remains there during a transit time τ_b , allowing exchanges to take place, and finally carried away and replaced by the same amount of blood. This phenomenon is periodically reproduced each time period τ_b . The dynamics of the gas exchange within the time interval $(0, \tau_b)$ through the alveolo-capillary barrier is modelled by a simple mole balance: $V_c \mathcal{C}_{\text{O}_2}(P_{\text{O}_2}, P_{\text{CO}_2})$ and $V_c \mathcal{C}_{\text{CO}_2}(P_{\text{O}_2}, P_{\text{CO}_2})$ correspond to the number of moles of oxygen and carbon dioxide in the capillary volume and their variations only depend on the pressure drop through the barrier. At each time t , we consider an auxiliary system describing this dynamics by introducing an auxiliary time variable $\theta \in (0, \tau_b)$ directly related to blood, and not to the respiration time. This dynamical process is illustrated on Figure 3, and at every time t , we solve

$$(10) \quad \begin{cases} V_c \frac{d}{d\theta} (\mathcal{C}_{\text{O}_2}(P_{\text{O}_2}(t, \theta), P_{\text{CO}_2}(t, \theta))) &= D_{m, \text{O}_2} (\chi_{\text{O}_2}(t) P_{\text{atm}} - P_{\text{O}_2}(t, \theta)), \\ V_c \frac{d}{d\theta} (\mathcal{C}_{\text{CO}_2}(P_{\text{O}_2}(t, \theta), P_{\text{CO}_2}(t, \theta))) &= D_{m, \text{CO}_2} (\chi_{\text{CO}_2}(t) P_{\text{atm}} - P_{\text{CO}_2}(t, \theta)), \end{cases} \quad \theta \in (0, \tau_b).$$

This system has to be supplemented with initial conditions. At every time t , deoxygenated blood arrives, so that we take as initial conditions

$$(11) \quad P_{\text{O}_2}(t, 0) = P_{\text{O}_2}^v, \quad P_{\text{CO}_2}(t, 0) = P_{\text{CO}_2}^v,$$

where $P_{\text{O}_2}^v, P_{\text{CO}_2}^v$ are the deoxygenated blood pressures of oxygen and carbon dioxide (blood poor in oxygen and rich in carbon dioxide) entering the lung before the gaseous exchanges. We emphasize that t here acts as a parameter, and, at every time t , the above system (10)–(11) must be solved for $\theta \in (0, \tau_b)$.

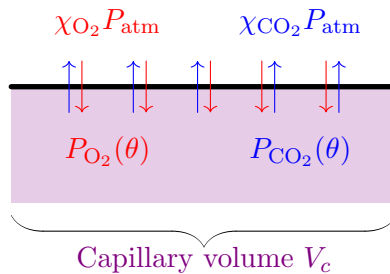


FIGURE 3. Schematic view of the dynamical process within the time interval $(0, \tau_b)$.

We are now in a position to properly determine the instantaneous average fluxes $q_{\text{O}_2}(t)$ and $q_{\text{CO}_2}(t)$ at each time t through an averaging process over a time interval $(0, \tau_b)$, that is

$$q_{\text{O}_2}(t) = \frac{1}{\tau_b} \int_0^{\tau_b} D_{m, \text{O}_2} (\chi_{\text{O}_2}(t) P_{\text{atm}} - P_{\text{O}_2}(t, \theta)) d\theta,$$

$$q_{\text{CO}_2}(t) = \frac{1}{\tau_b} \int_0^{\tau_b} D_{m,\text{CO}_2} (\chi_{\text{CO}_2}(t) P_{\text{atm}} - P_{\text{CO}_2}(t, \theta)) d\theta.$$

Thanks to (10), the fluxes can be rewritten as

$$(12) \quad q_{\text{O}_2}(t) = \frac{V_c}{\tau_b} [\mathcal{C}_{\text{O}_2}(P_{\text{O}_2}(t, \tau_b), P_{\text{CO}_2}(t, \tau_b)) - \mathcal{C}_{\text{O}_2}(P_{\text{O}_2}(t, 0), P_{\text{CO}_2}(t, 0))],$$

$$(13) \quad q_{\text{CO}_2}(t) = \frac{V_c}{\tau_b} [\mathcal{C}_{\text{CO}_2}(P_{\text{O}_2}(t, \tau_b), P_{\text{CO}_2}(t, \tau_b)) - \mathcal{C}_{\text{CO}_2}(P_{\text{O}_2}(t, 0), P_{\text{CO}_2}(t, 0))].$$

In this model, $P_{\text{O}_2}(t, \tau_b)$ and $P_{\text{CO}_2}(t, \tau_b)$ represent the instantaneous oxygenated blood pressures at time t and thus are the surrogates of the arterial blood pressures. We hence shall denote, from now on,

$$(14) \quad P_{\text{O}_2}^a(t) = P_{\text{O}_2}(t, \tau_b), \quad P_{\text{CO}_2}^a(t) = P_{\text{CO}_2}(t, \tau_b).$$

Taking into account (11) and (14) in (12)–(13), we get, for any t ,

$$(15) \quad q_{\text{O}_2}(t) = \frac{V_c}{\tau_b} [\mathcal{C}_{\text{O}_2}(P_{\text{O}_2}^a(t), P_{\text{CO}_2}^a(t)) - \mathcal{C}_{\text{O}_2}(P_{\text{O}_2}^v, P_{\text{CO}_2}^v)],$$

$$(16) \quad q_{\text{CO}_2}(t) = \frac{V_c}{\tau_b} [\mathcal{C}_{\text{CO}_2}(P_{\text{O}_2}^a(t), P_{\text{CO}_2}^a(t)) - \mathcal{C}_{\text{CO}_2}(P_{\text{O}_2}^v, P_{\text{CO}_2}^v)].$$

The following situations can happen for the exchange dynamics at the alveolar-capillary interface:

- $P_{\text{O}_2}^a(t) \simeq \chi_{\text{O}_2}(t) P_{\text{atm}}$, $P_{\text{CO}_2}^a(t) \simeq \chi_{\text{CO}_2}(t) P_{\text{atm}}$ in healthy situations (for which equilibrium between the alveolar partial pressures and the blood partial pressures is reached for both gases during the transit time);
- if kinetic limitation occurs, $P_{\text{O}_2}^a(t) < \chi_{\text{O}_2}(t) P_{\text{atm}}$ (same for CO_2), and the equilibrium is not reached during the transit time, which can happen for several pathologies.

Yet, in both cases, the corresponding O_2 and CO_2 transfer rates are given by (15)–(16).

Remark 2. *The use of the auxiliary time variable θ may in fact be reinterpreted as a one-dimensional space averaging process all along the capillary path. Indeed, introducing \bar{u} as the mean blood velocity in the capillary volume and $\bar{\ell}$ as the mean length of the capillaries, τ_b satisfies $\tau_b = \bar{\ell}/\bar{u}$. We can introduce the one-dimensional space variable $x \in (0, \bar{\ell})$ as $x = \bar{u}\theta$, which maps the capillary path from the entrance of the capillaries (with deoxygenated blood) to their exit (with oxygenated blood). Defining $\tilde{P}_{\text{O}_2}(t, x) = P_{\text{O}_2}(t, \theta)$ and $\tilde{P}_{\text{CO}_2}(t, x) = P_{\text{CO}_2}(t, \theta)$, equations (10) become, for every t ,*

$$\begin{cases} V_c \bar{u} \frac{d}{dx} (\mathcal{C}_{\text{O}_2}(\tilde{P}_{\text{O}_2}(t, x), \tilde{P}_{\text{CO}_2}(t, x))) &= D_{m,\text{O}_2} (\chi_{\text{O}_2}(t) P_{\text{atm}} - \tilde{P}_{\text{O}_2}(t, x)), \\ V_c \bar{u} \frac{d}{dx} (\mathcal{C}_{\text{CO}_2}(\tilde{P}_{\text{O}_2}(t, x), \tilde{P}_{\text{CO}_2}(t, x))) &= D_{m,\text{CO}_2} (\chi_{\text{CO}_2}(t) P_{\text{atm}} - \tilde{P}_{\text{CO}_2}(t, x)), \end{cases} \quad x \in (0, \bar{\ell}),$$

with the condition at the entrance of the capillaries

$$\tilde{P}_{\text{O}_2}(t, 0) = P_{\text{O}_2}^v, \quad \tilde{P}_{\text{CO}_2}(t, 0) = P_{\text{CO}_2}^v.$$

Using the space variable x , the instantaneous average fluxes are given, for every t , by

$$\begin{aligned} q_{\text{O}_2}(t) &= \frac{V_c \bar{u}}{\bar{\ell}} [\mathcal{C}_{\text{O}_2}(\tilde{P}_{\text{O}_2}(t, \bar{\ell}), \tilde{P}_{\text{CO}_2}(t, \bar{\ell})) - \mathcal{C}_{\text{O}_2}(\tilde{P}_{\text{O}_2}(t, 0), \tilde{P}_{\text{CO}_2}(t, 0))], \\ q_{\text{CO}_2}(t) &= \frac{V_c \bar{u}}{\bar{\ell}} [\mathcal{C}_{\text{CO}_2}(\tilde{P}_{\text{O}_2}(t, \bar{\ell}), \tilde{P}_{\text{CO}_2}(t, \bar{\ell})) - \mathcal{C}_{\text{CO}_2}(\tilde{P}_{\text{O}_2}(t, 0), \tilde{P}_{\text{CO}_2}(t, 0))], \end{aligned}$$

which correspond to (12)–(13), the analogous of equation (14) being

$$P_{\text{O}_2}^a(t) = \tilde{P}_{\text{O}_2}(t, \bar{\ell}), \quad P_{\text{CO}_2}^a(t) = \tilde{P}_{\text{CO}_2}(t, \bar{\ell}).$$

Consequently, using the one-dimensional space variable x instead of the auxiliary time variable θ provides the very same computation of the instantaneous average fluxes, and the formalism can be interpreted as an averaging process in space along the capillary path. Figure 4 illustrates this dynamics.

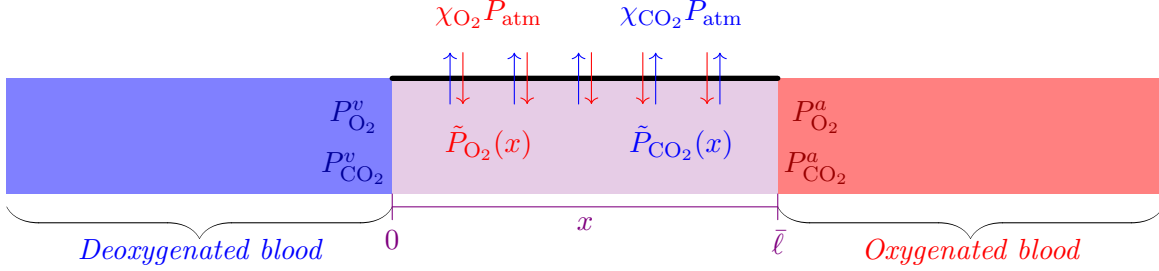


FIGURE 4. Schematic view of the gas transfer along the capillary path.

Remark 3. The arterial blood pressures $P_{O_2}^a(t)$ and $P_{CO_2}^a(t)$ may be viewed as functions of the unknowns $\chi_{O_2}(t)$ and $\chi_{CO_2}(t)$ and the gas exchange parameters D_{m,O_2} , D_{m,CO_2} , V_c , τ_b , $P_{O_2}^v$, $P_{CO_2}^v$. Hence, they could be computed for suitable ranges of these quantities, leading to tabulated values of $P_{O_2}^a$ and $P_{CO_2}^a$.

Remark 4. From the numerical viewpoint, it is useful to notice that (10) can be formally written as

$$\begin{cases} \frac{d}{dt}(F(u, v)) = f(u), \\ \frac{d}{dt}(G(u, v)) = g(v), \end{cases}$$

with initial data for u and v . Thus we get

$$\begin{cases} \partial_u F(u, v)\dot{u} + \partial_v F(u, v)\dot{v} = f(u), \\ \partial_u G(u, v)\dot{u} + \partial_v G(u, v)\dot{v} = g(v), \end{cases}$$

so that

$$\begin{cases} \dot{u} = \frac{\partial_v G(u, v)f(u) - \partial_v F(u, v)g(v)}{\partial_u F(u, v)\partial_v G(u, v) - \partial_v F(u, v)\partial_u G(u, v)}, \\ \dot{v} = -\frac{\partial_u G(u, v)f(u) - \partial_u F(u, v)g(v)}{\partial_u F(u, v)\partial_v G(u, v) - \partial_v F(u, v)\partial_u G(u, v)}, \end{cases}$$

if the denominator is non-zero. It will be the case for the parameter ranges and the functions F and G which we shall deal with.

2.4. Summary of the 0D model. As a consequence, the mechanical and gas exchange model is written as a nonlinear first-order differential system governing the behaviour of three observable quantities ($t \mapsto V(t)$, $t \mapsto \chi_{O_2}(t)$ and $t \mapsto \chi_{CO_2}(t)$). It also requires to compute q_{O_2} , q_{CO_2} and auxiliary quantities $P_{O_2}^a$, $P_{CO_2}^a$, at each time t . Let us summarize the whole dynamical system

which we consider, *i.e.* equations (1)–(3), (7)–(11), and (14)–(16)

Mechanical model

$$\dot{V}(t) = -\frac{1}{\tau}(V(t) - \text{FRC}) + \frac{1}{R}P_{\text{ext}}(t), \quad \text{where } \tau = \frac{R}{E}$$

Balance of gases in the lung volume during each respiratory cycle $[kT, (k+1)T]$

$$\dot{\chi}_{\text{O}_2}(t) = \frac{1}{V(t) - V_D} \left[(1 - \phi(t)) \dot{V} (\chi_{\text{O}_2}^{\text{atm}}(t) - \chi_{\text{O}_2}(t)) \mathbb{1}_{\mathbb{R}_+}(\dot{V}(t)) - q_{\text{O}_2}(t) \right]$$

$$\dot{\chi}_{\text{CO}_2}(t) = \frac{1}{V(t) - V_D} \left[(1 - \phi(t)) \dot{V} (\chi_{\text{CO}_2}^{\text{atm}}(t) - \chi_{\text{CO}_2}(t)) \mathbb{1}_{\mathbb{R}_+}(\dot{V}(t)) - q_{\text{CO}_2}(t) \right]$$

where $V_D = V_D^A + \max(V(kT) - \text{FRC}, 0)$ and $\phi(t) = V_D / (V(t) - V(kT) + V_D)$

Instantaneous gas fluxes through the alveolo-capillary membrane

$$q_{\text{O}_2}(t) = \frac{V_c}{\tau_b} (\mathcal{C}_{\text{O}_2}(P_{\text{O}_2}^a(t), P_{\text{CO}_2}^a(t)) - \mathcal{C}_{\text{O}_2}(P_{\text{O}_2}^v, P_{\text{CO}_2}^v))$$

$$q_{\text{CO}_2}(t) = \frac{V_c}{\tau_b} (\mathcal{C}_{\text{CO}_2}(P_{\text{O}_2}^a(t), P_{\text{CO}_2}^a(t)) - \mathcal{C}_{\text{CO}_2}(P_{\text{O}_2}^v, P_{\text{CO}_2}^v))$$

Instantaneous partial pressures in arterial blood

$(P_{\text{O}_2}^a(t), P_{\text{CO}_2}^a(t)) = (P_{\text{O}_2}(t, \tau_b), P_{\text{CO}_2}(t, \tau_b))$, where $\theta \mapsto (P_{\text{O}_2}(t, \theta), P_{\text{CO}_2}(t, \theta))$ solves

$$\left\{ \begin{array}{ll} V_c \frac{d}{d\theta} (\mathcal{C}_{\text{O}_2}(P_{\text{O}_2}(t, \theta), P_{\text{CO}_2}(t, \theta))) &= D_{m, \text{O}_2} (\chi_{\text{O}_2}(t) P_{\text{atm}} - P_{\text{O}_2}(t, \theta)), \quad \theta \in (0, \tau_b) \\ V_c \frac{d}{d\theta} (\mathcal{C}_{\text{CO}_2}(P_{\text{O}_2}(t, \theta), P_{\text{CO}_2}(t, \theta))) &= D_{m, \text{CO}_2} (\chi_{\text{CO}_2}(t) P_{\text{atm}} - P_{\text{CO}_2}(t, \theta)), \quad \theta \in (0, \tau_b) \\ P_{\text{O}_2}(t, 0) &= P_{\text{O}_2}^v, \\ P_{\text{CO}_2}(t, 0) &= P_{\text{CO}_2}^v. \end{array} \right.$$

This system is supplemented with initial conditions on V , χ_{O_2} and χ_{CO_2} , and the functions \mathcal{C}_{O_2} and $\mathcal{C}_{\text{CO}_2}$ are defined in the next section, see (21) and (24). Recall that \mathcal{C}_{O_2} and $\mathcal{C}_{\text{CO}_2}$ are nonlinear functions inducing a coupling between oxygen and carbon dioxide dynamics (Bohr and Haldane effects). As already stated, the determination of instantaneous partial pressures in arterial blood requires to solve the last system at each time step.

Furthermore, the system is completely driven by the muscle command $t \mapsto P_{\text{ext}}(t)$. The parameters, which can be fitted to mimic pathologies, are the resistance of the bronchial tree (which may be increased, for instance, to model asthma), the elastance of the lung parenchyma (which could be changed in fibrosis or emphysema modelling), the diffusion parameters (which could be decreased in infectious diseases). The parameters R and E have a direct impact on the ventilation process, and thus on the dynamic of lung volume and available fresh air, whereas the parameters D_m play a crucial role in the gas diffusion. Note that V_c and τ_b are two other constants which can be fitted to take into account some haemodynamic changes.

3. GAS EXCHANGE MODEL FOR OXYGEN AND CARBON DIOXIDE

In this section, we focus on the coupled diffusion process involving oxygen and carbon dioxide through the so-called Bohr and Haldane effects, in order to define the functions \mathcal{C}_{O_2} and $\mathcal{C}_{\text{CO}_2}$.

3.1. Balance of oxygen including the Bohr effect. In order to describe the oxygen concentration in the blood and take into account the Bohr effect, we adapt the model developped in [19, Sn. 2] by including the dependency of the O_2 saturation with respect to CO_2 .

Classically, the oxygen concentration in blood plasma can be expressed in terms of the oxygen partial pressure as σP_{O_2} , where $\sigma = 1.4 \cdot 10^{-6} \text{ mol} \cdot \text{L}^{-1} \cdot \text{mmHg}^{-1}$ denotes the oxygen solubility in the

plasma. To this oxygen concentration in plasma, one must add a significant contribution due to the capture of some O_2 by hemoglobin (Hb). This latter contribution is written as $4C_{Hb}\mathcal{H}_0(P_{O_2})$, where C_{Hb} is the total concentration of hemoglobin (in both native and combined forms), $\mathcal{H}_0 : \mathbb{R}_+ \rightarrow [0, 1]$ allows to quantify the hemoglobin saturation, and 4 is the maximal number of oxygen molecules that a hemoglobin molecule may carry. The saturation function \mathcal{H}_0 [14, 34] is often referred to as *Hill's* or *oxygen dissociation curve*, and can be expressed as

$$(17) \quad \mathcal{H}_0(P_{O_2}) = \frac{P_{O_2}^{2.5}}{P_0^{2.5} + P_{O_2}^{2.5}},$$

where $P_0 = 26$ mmHg, see [14] and Figure 5. The oxygen concentration in the blood in both forms (free and captured by hemoglobin) is then written as

$$(18) \quad \mathcal{C}_{O_2}(P_{O_2}) = \sigma P_{O_2} + 4C_{Hb}\mathcal{H}_0(P_{O_2}).$$

This simple model allows to recover, without tuning up any parameter, the order of magnitude of the oxygen transfer rate at rest [10, 32, 33] for healthy situations, namely $q_{O_2} = 250 \text{ mL} \cdot \text{min}^{-1}$, see [19].

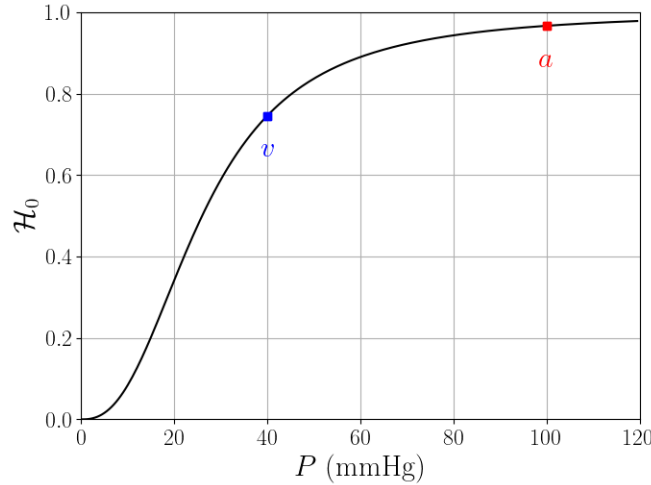


FIGURE 5. Oxygen dissociation curve: in standard conditions, venous blood is poor in oxygen ($P_{O_2}^v = 40$ mmHg, corresponding to Hb saturation at 75%) whereas arterial blood has been enriched in O_2 , through the diffusion process during the travel in the capillary ($P_{O_2}^a = 100$ mmHg, corresponding to Hb saturation at 97.5%).

Nevertheless, the Bohr effect is still not taken into account in (18), since the expression of \mathcal{C}_{O_2} does not depend on P_{CO_2} . In fact, the oxygen dissociation curve, and hence the total concentration of oxygen in the blood, depends on several factors, such as pH, P_{CO_2} , temperature, *etc.* Here, we choose to include in our model not only the influence of P_{CO_2} , but also the one of pH, and to neglect the temperature influence: we replace the classical Hill curve \mathcal{H}_0 by

$$P_{O_2} \mapsto \mathcal{H}(P_{O_2}, P_{CO_2}, \text{pH}).$$

The expression of $\mathcal{H}(P_{O_2}, P_{CO_2}, \text{pH})$ can be built by considering the following modification, proposed in [15]:

$$(19) \quad \mathcal{H}(P_{O_2}, P_{CO_2}, \text{pH}) = \mathcal{H}_0(\mathcal{P}(P_{O_2}, P_{CO_2}, \text{pH}))$$

$$(20) \quad \mathcal{P}(P_{O_2}, P_{CO_2}, \text{pH}) = P_{O_2} \cdot 10^{0.40 \cdot (\text{pH} - 7.4) + 0.06 \cdot (\log_{10}(40) - \log_{10}(P_{CO_2}))}.$$

Here, (20) includes a correction factor which accounts for the variations of pH and P_{CO_2} and their distances to their reference values in healthy situations, namely 7.4 for the average blood pH, and 40 mmHg for the standard average carbon dioxide arterial blood partial pressure. Hence, the new expression of \mathcal{C}_{O_2} is given by

$$(21) \quad \begin{aligned} \mathcal{C}_{\text{O}_2}(P_{\text{O}_2}, P_{\text{CO}_2}, \text{pH}) &= \sigma P_{\text{O}_2} + 4C_{\text{Hb}} \mathcal{H}(P_{\text{O}_2}, P_{\text{CO}_2}, \text{pH}) \\ &= \sigma P_{\text{O}_2} + 4C_{\text{Hb}} \mathcal{H}_0 \left(P_{\text{O}_2} \cdot 10^{0.40 \cdot (\text{pH} - 7.4) + 0.06 \cdot (\log_{10}(40) - \log_{10}(P_{\text{CO}_2}))} \right), \end{aligned}$$

where \mathcal{H}_0 is the standard Hill curve defined by (17).

Remark 5. *One could also eliminate pH as a given parameter and take into account the acid-base equilibrium. The study of the acid-base $\text{CO}_2/\text{HCO}_3^-$ is described in [34, Chap. 6, pp. 96–101] and leads to*

$$(22) \quad \text{pH} = \text{p}K_A + \log_{10} \frac{C_{\text{HCO}_3^-}}{0.03 \cdot P_{\text{CO}_2}},$$

where $\text{p}K_A = 6.1$ is the dissociation constant of carbonic acid and $C_{\text{HCO}_3^-}$ denotes the bicarbonate concentration in the blood, expressed in $\text{mmol} \cdot \text{L}^{-1}$. This concentration is mainly regulated by the kidney and its normal value lies between $22 \text{ mmol} \cdot \text{L}^{-1}$ and $26 \text{ mmol} \cdot \text{L}^{-1}$. The normal bicarbonate concentration in the oxygenated blood is around $24 \text{ mmol} \cdot \text{L}^{-1}$, whereas it is $26 \text{ mmol} \cdot \text{L}^{-1}$ for deoxygenated blood. It means in particular that, first, the default value of pH in the oxygenated blood is 7.4 as expected and, second, as long as the ratio between $C_{\text{HCO}_3^-}$ and $0.03 \cdot P_{\text{CO}_2}$ equals 20, the value of pH remains at 7.4.

In this case, the expression of the oxygen concentration with respect to the partial pressures of oxygen and carbon dioxide would be given by

$$(23) \quad \tilde{\mathcal{C}}_{\text{O}_2}(P_{\text{O}_2}, P_{\text{CO}_2}, C_{\text{HCO}_3^-}) = \sigma P_{\text{O}_2} + 4C_{\text{Hb}} \mathcal{H} \left(P_{\text{O}_2}, P_{\text{CO}_2}, 6.10 + \log_{10} \frac{C_{\text{HCO}_3^-}}{0.03 \cdot P_{\text{CO}_2}} \right),$$

where \mathcal{H} is defined by (19).

In the next paragraphs, we study the influence of pH and P_{CO_2} on the oxygen dissociation curves.

Influence of pH for a fixed value of P_{CO_2} . On Figure 6a, the function $P_{\text{O}_2} \mapsto \mathcal{H}(P_{\text{O}_2}, P_{\text{CO}_2}, \text{pH})$ is plotted for $P_{\text{CO}_2} = 40 \text{ mmHg}$ (arterial blood partial pressure in a healthy regime) and different values of pH (including extremal ones which do not correspond to standard physiological regimes). Note that the profile of $P_{\text{O}_2} \mapsto \mathcal{H}(P_{\text{O}_2}, P_{\text{CO}_2}, \text{pH})$ for $P_{\text{CO}_2} = 46 \text{ mmHg}$ (venous blood partial pressure in a healthy regime) is roughly identical. Actually, only little difference is observed when P_{CO_2} is set in the whole interval (5, 80). Consequently, for a fixed value of P_{CO_2} , the chosen oxygen dissociation curve is not very sensitive to pH.

Influence of P_{CO_2} for a fixed value of pH. The function $P_{\text{O}_2} \mapsto \mathcal{H}(P_{\text{O}_2}, P_{\text{CO}_2}, \text{pH})$ is described for $\text{pH} = 7.4$ on Figure 6b. We observe that the oxygen dissociation curve is not deeply impacted by the variations of P_{CO_2} . The sensitivity of the curve with respect to P_{CO_2} is really low.

3.2. Balance of carbon dioxide including the Haldane effect. The carbon dioxide concentration in the blood is determined by its different forms, as CO_2 is carried in the blood under three forms: dissolved, after a chemical reaction, that implies hemoglobin, as bicarbonate, and in combination with proteins as carbamino compounds. The major quantity of carbon dioxide reacts with hemoglobin which fixes H^+ ions and leads to the bicarbonate creation. This binding gives rise to the Haldane effect, where blood deoxygenation increases its ability to carry H^+ , see [34]: the presence of reduced hemoglobin in the peripheral blood helps with the CO_2 loading, whereas the oxygenation occurring in the pulmonary capillary supports the unloading. The relationship between the partial

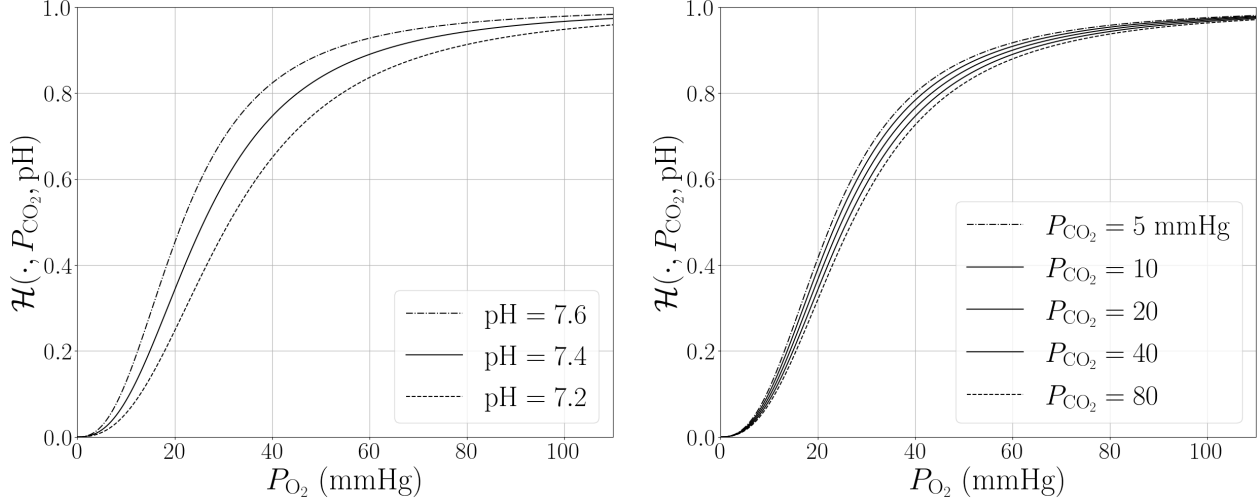


FIGURE 6. Oxygen dissociation curves $P_{\text{O}_2} \mapsto \mathcal{H}(P_{\text{O}_2}, P_{\text{CO}_2}, \text{pH})$ for (a) $P_{\text{CO}_2} = 40$ mmHg and various pH, and (b) pH = 7.4 and various values of P_{CO_2} .

pressure of CO_2 and the total CO_2 concentration in the blood (in all forms) is often referred to as the carbon dioxide dissociation curve, and it is much more linear than is the oxygen dissociation curve, at least in standard regimes.

Actually, as pointed out e.g. in [34], because of the Haldane effect, the exchange dynamics of CO_2 is strongly influenced by the dynamics of O_2 , as oxygenated blood carries less carbon dioxide for the same oxygen partial pressure. In terms of mathematical modelling, it means that the function $\mathcal{C}_{\text{CO}_2}$, which models the concentration of CO_2 in the blood in all forms, highly depends on the partial pressure of O_2 . Several phenomenological formulas have been proposed in the literature to account for this phenomenon, see [17, 18] for instance. We choose to use here, for the sake of simplicity, the Meade formula [21], giving the concentration in $\text{mol} \cdot \text{L}^{-1}$

$$(24) \quad \mathcal{C}_{\text{CO}_2}(P_{\text{O}_2}, P_{\text{CO}_2}) = \frac{10^{-3}}{V_m} (463 e^{0.00415 P_{\text{CO}_2}} - 340 e^{-0.0445 P_{\text{CO}_2}} + 62(0.975 - \mathcal{H}_0(P_{\text{O}_2}))),$$

where \mathcal{H}_0 is the oxygen Hill function defined by (17) and V_m the molar volume of an ideal gas at standard temperature and pressure, namely $V_m = 22.4 \text{ L} \cdot \text{mol}^{-1}$. The dependence with respect to pH is not taken into account. Note that this fitted formula may not be the most accurate but it illustrates the Haldane effect and the strong coupling between O_2 and CO_2 .

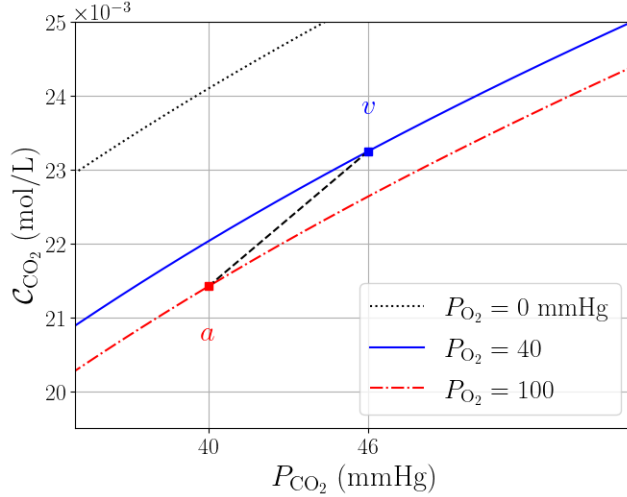
Figure 7 represents the function $P_{\text{CO}_2} \mapsto \mathcal{C}_{\text{CO}_2}(P_{\text{O}_2}, P_{\text{CO}_2})$ for three values of P_{O_2} , namely 0, 40 and 100 mmHg, the last two corresponding to venous and arterial oxygen partial pressures in healthy situations.

3.3. Quantitative study of the coupled diffusion process. Thanks to (21) for the oxygen concentration with Bohr's effect, and (24) for the carbon dioxide concentration with Haldane's, we can estimate the neat transfer rate for both O_2 and CO_2 . We consider the following standard values for the venous and arterial partial pressures

$$(25) \quad \begin{aligned} P_{\text{O}_2}^v &= 40 \text{ mmHg}, & P_{\text{CO}_2}^v &= 46 \text{ mmHg}, \\ P_{\text{O}_2}^a &= 100 \text{ mmHg}, & P_{\text{CO}_2}^a &= 40 \text{ mmHg}. \end{aligned}$$

Based on (21) and Table 16 from Appendix A, the oxygen transfer rate can be estimated by

$$q_{\text{O}_2} = \frac{V_c}{\tau_b} (\mathcal{C}_{\text{O}_2}(P_{\text{O}_2}^a, P_{\text{CO}_2}^a, 7.4) - \mathcal{C}_{\text{O}_2}(P_{\text{O}_2}^v, P_{\text{CO}_2}^v, 7.4)) = 1.92 \cdot 10^{-4} \text{ mol} \cdot \text{s}^{-1},$$

FIGURE 7. Carbon dioxide dissociation curve $P_{\text{CO}_2} \mapsto \mathcal{C}_{\text{CO}_2}(P_{\text{O}_2}, P_{\text{CO}_2})$.

or, involving the molar volume V_m of an ideal gas, we get

$$q_{\text{O}_2} = 258 \text{ mL} \cdot \text{min}^{-1}.$$

We can also estimate the transfer rate of CO_2 , based on (24), as

$$q_{\text{CO}_2} = \frac{V_c}{\tau_b} (\mathcal{C}_{\text{CO}_2}(P_{\text{O}_2}^a, P_{\text{CO}_2}^a) - \mathcal{C}_{\text{CO}_2}(P_{\text{O}_2}^v, P_{\text{CO}_2}^v)) = -1.70 \cdot 10^{-4} \text{ mol} \cdot \text{s}^{-1},$$

or, using again V_m ,

$$q_{\text{CO}_2} = -228 \text{ mL} \cdot \text{min}^{-1}.$$

The standard values of the fluxes are respectively around $250 \text{ mL} \cdot \text{min}^{-1}$ for the oxygen, and around $-200 \text{ mL} \cdot \text{min}^{-1}$ for the carbon dioxide. We observe that, compared to those standard values, the computations from (21) and (24) give the same order of magnitude. Moreover, note that if we compute the associated respiratory quotient, denoted by RQ and defined as $|q_{\text{CO}_2}/q_{\text{O}_2}|$, we obtain $\text{RQ} = 0.884$, which also lies in the standard range for this ratio.

Remark 6. *At rest, the Bohr and Haldane effects do not seem to have the same importance in healthy regimes (with $(P_{\text{O}_2}^v, P_{\text{CO}_2}^v) = (40, 46)$ and $(P_{\text{O}_2}^a, P_{\text{CO}_2}^a) = (100, 40)$, all values given in mmHg), see [11, 9, 10, 18]. In the static regime, neglecting the Haldane effect produces a sharp reduction of the carbon dioxide flux (-37%), whereas the Bohr effect seems totally negligible, since it has no effect of the oxygen flux.*

Remark 7. *When taking into account the bicarbonate concentration instead of pH, based on (23), remembering that $C_{\text{HCO}_3^-} = 24 \text{ mmol} \cdot \text{L}^{-1}$, we obtain*

$$q_{\text{O}_2} = \frac{V_c}{\tau_b} (\tilde{\mathcal{C}}_{\text{O}_2}(P_{\text{O}_2}^a, P_{\text{CO}_2}^a, 24) - \tilde{\mathcal{C}}_{\text{O}_2}(P_{\text{O}_2}^v, P_{\text{CO}_2}^v, 24)) = 2.15 \cdot 10^{-4} \text{ mol} \cdot \text{s}^{-1},$$

or, using V_m ,

$$q_{\text{O}_2} = 289 \text{ mL} \cdot \text{min}^{-1}.$$

The associated respiratory quotient is then $\text{RQ} = 0.789$, which remains in the standard range.

Let us now investigate the possible diffusion limitation by solving a dynamical system, similar to (10), satisfied by the oxygen and carbon dioxide blood partial pressures, for different values of

the diffusion coefficients. This system is written as

$$(26) \quad \begin{cases} V_c \frac{d}{d\theta} (C_{O_2}(P_{O_2}, P_{CO_2}, \text{pH})) &= D_{m,O_2} (P_{O_2}^{\text{alv}} - P_{O_2}), & \theta \in (0, \tau_b), \\ V_c \frac{d}{d\theta} (C_{CO_2}(P_{O_2}, P_{CO_2})) &= D_{m,CO_2} (P_{CO_2}^{\text{alv}} - P_{CO_2}), & \theta \in (0, \tau_b), \\ P_{O_2}(0) &= P_{O_2}^v, \\ P_{CO_2}(0) &= P_{CO_2}^v, \end{cases}$$

where $P_{O_2}^{\text{alv}}$ and $P_{CO_2}^{\text{alv}}$ are the gas partial pressures in the alveolar compartment, and pH is set at 7.4. We define the following reference situation:

- the gas partial pressures in the venous blood are chosen as in (25);
- the gas partial pressures in the alveolar compartment are chosen equal to the arterial reference values given in (25);
- the membrane is healthy, *i.e.*

$$\begin{aligned} D_{m,O_2}^h &= 21 \text{ mL} \cdot \text{min}^{-1} \cdot \text{mmHg}^{-1}, \\ D_{m,CO_2}^h &= 20 D_{m,O_2}^h = 420 \text{ mL} \cdot \text{min}^{-1} \cdot \text{mmHg}^{-1}. \end{aligned}$$

We then investigate three different values of the diffusion coefficients: $D_m = D_m^h$, $D_m = D_m^h/2$ and $D_m = D_m^h/4$, D_{m,CO_2} remaining equal to $20D_{m,O_2}$. The other parameters are set to their reference values, see Table 16.

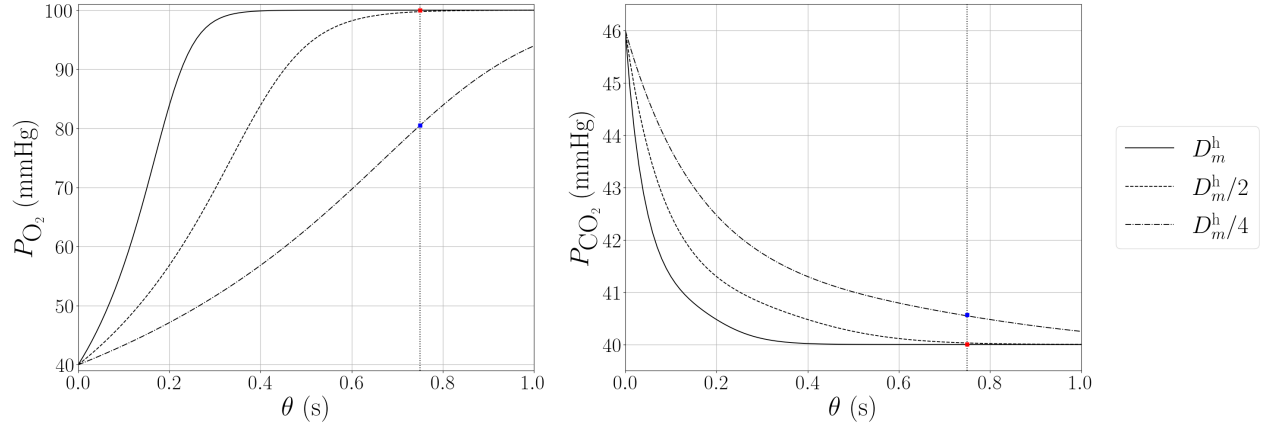


FIGURE 8. Dynamics of the gas exchange through the alveolo-capillary membrane: $\theta \mapsto P_{O_2}(\theta)$ and $\theta \mapsto P_{CO_2}(\theta)$.

The time evolution of the partial pressures of both gases on Figure 8 illustrates the kinetic limitation phenomenon. It allows to highlight several observations.

First, in the reference healthy regime, partial pressures evolve from the venous (or deoxygenated) value to the alveolar one. Equilibrium is reached within the available time $\tau_b = 0.75$ s and it has some robustness since the time needed to obtain this balance is about the third of τ_b .

Second, in a moderately impaired regime, e.g. $D_m = D_m^h/2$ for both species, we observe that the equilibrium between partial pressures is reached around time τ_b , *i.e.*

$$P_{O_2}^a \simeq P_{O_2}^{\text{alv}}, \quad P_{CO_2}^a \simeq P_{CO_2}^{\text{alv}},$$

even if the gas exchange dynamics has been slowed down by the membrane impairment. This impairment is not sufficient to deteriorate the gas transfer: q_{O_2} and q_{CO_2} have the same values as in the healthy case.

Last, in a severely impaired regime, here $D_m = D_m^h/4$ for both gases, we observe that the equilibrium between partial pressures is not reached. As a consequence, we have

$$P_{O_2}^a < P_{O_2}^{alv}, \quad P_{CO_2}^a > P_{CO_2}^{alv},$$

and the neat transfer of gases, for both O_2 and CO_2 , is lowered, compared to the healthy situation.

In the above example, the possible kinetic limitation has been illustrated by considering different values of the diffusing membrane. Note that the kinetic limitation may also occur in other situations: if τ_b is significantly reduced and V_c is increased (e.g. during exercise), it may drop below the time necessary to achieve equilibrium between the partial pressures.

In the following sections, we present various numerical studies. We start by illustrating our model behaviour for a healthy patient in two cases: standard respiration and hyperventilation. Starting from this reference situation, we investigate the model sensitivity, with respect to the physical parameters of resistance, elastance and diffusion coefficients of the alveolo-capillary membrane, of two types of characteristic outputs, the alveolo-capillary fluxes and the oxygenated blood partial pressures. More precisely, we explore whether there exist global structures in the input parameters and study their crossed sensitivity. Eventually, we try to recover known qualitative behaviours by varying the various physical parameters to mimic pathological situations such as asthma, emphysema...

4. HEALTHY REFERENCE RESPIRATION SCENARIOS

We first investigate a healthy situation within a normal respiration framework. The mechanical parameters are set to

$$(27) \quad R^h = 2 \text{ cmH}_2\text{O} \cdot \text{L}^{-1} \cdot \text{s}, \quad E^h = 3.5 \text{ cmH}_2\text{O} \cdot \text{L}^{-1},$$

so that the relaxation time $\tau^h = R^h/E^h$ associated to the mechanical model (1) equals 0.57 s. For the dead space volume (2), we recall the standard value of the anatomical dead space for a healthy man $V_D^A = 0.15 \text{ L}$. For the diffusive model (10), we choose the same healthy values as in the previous section, which are

$$(28) \quad D_{m,O_2}^h = 21 \text{ mL} \cdot \text{min}^{-1} \cdot \text{mmHg}^{-1} = 1.6 \cdot 10^{-5} \text{ mol} \cdot \text{s}^{-1} \cdot \text{mmHg}^{-1},$$

$$(29) \quad D_{m,CO_2}^h = 20D_{m,O_2}^h = 420 \text{ mL} \cdot \text{min}^{-1} \cdot \text{mmHg}^{-1} = 3.2 \cdot 10^{-4} \text{ mol} \cdot \text{s}^{-1} \cdot \text{mmHg}^{-1}.$$

4.1. Normal breathing. We impose a periodic breathing scenario where the period T equals 5 s. The applied pressure P_{ext} is chosen piecewise constant, namely, in mmHg,

$$(30) \quad P_{\text{ext}}(t) = -2, \quad 0 \leq t < i_{\text{frac}}T, \quad P_{\text{ext}}(t) = 0, \quad i_{\text{frac}}T \leq t < T,$$

where the inspiration proportion i_{frac} is set to 0.35. In all the following tables, we list averaged quantities over a time period, denoted by $\langle \cdot \rangle$, while making sure periodic behaviour is approximately reached (more precisely, average over the last period for a final time $T_{\text{fin}} = 50 \text{ s}$). First, in this healthy situation, one can check that the values from Table 1 are standardly acknowledged.

TABLE 1. Averaged quantities in the healthy case with standard breathing parameters.

$\langle q_{O_2} \rangle$ (mL/min)	$\langle q_{CO_2} \rangle$ (mL/min)	RQ	$\langle P_{O_2}^a \rangle$ (mmHg)	$\langle P_{CO_2}^a \rangle$ (mmHg)	$\langle \chi_{O_2} \rangle$	$\langle \chi_{CO_2} \rangle$	V_D (L)	V_{\min} (L)	V_{\max} (L)
256	-203	0.793	97.6	41	13.7%	5.74%	0.152	2.50	3.05

Moreover, our quantities of interest evolve with respect to time as shown in Figures 9–11, on the last period before T_{fin} .

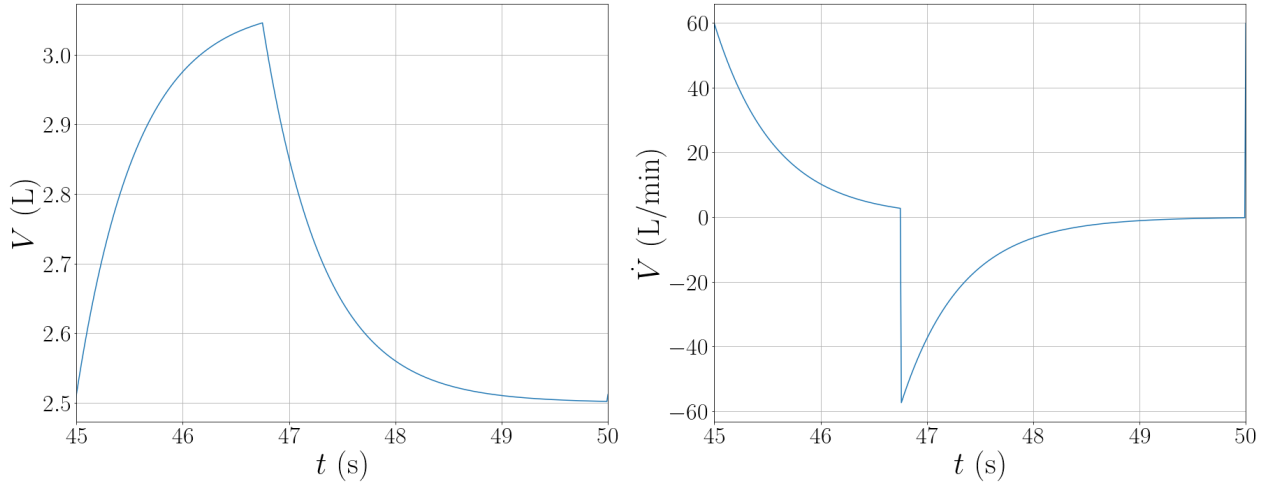


FIGURE 9. Plots w.r.t. time of (a) the total volume V and (b) the air flow \dot{V} .

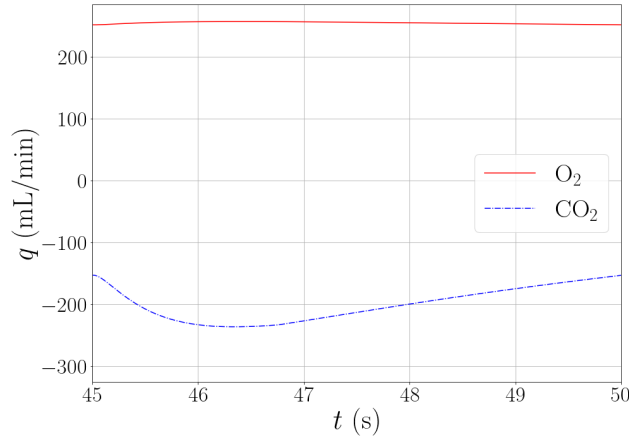


FIGURE 10. Plot w.r.t. time of the gaseous fluxes q_{O_2} and q_{CO_2} .

Remark 8. Note that, in this healthy situation, the extra pathological dead space V_D^P is negligible and the volume at the end of expiration almost equals FRC. Moreover, taking the anatomical dead space into account appears as crucial to recover the correct orders of magnitude of the physiological quantities. Indeed, when imposing $V_D = 0$, and subsequently $\phi = 0$ instead of (7), we obtain the gas exchange values given in Table 2, the dynamics of the lung respiratory volume remaining unchanged. Compared to Table 1, the impact of the dead space volume is especially clear for the carbon dioxide flux and the arterial blood partial pressure.

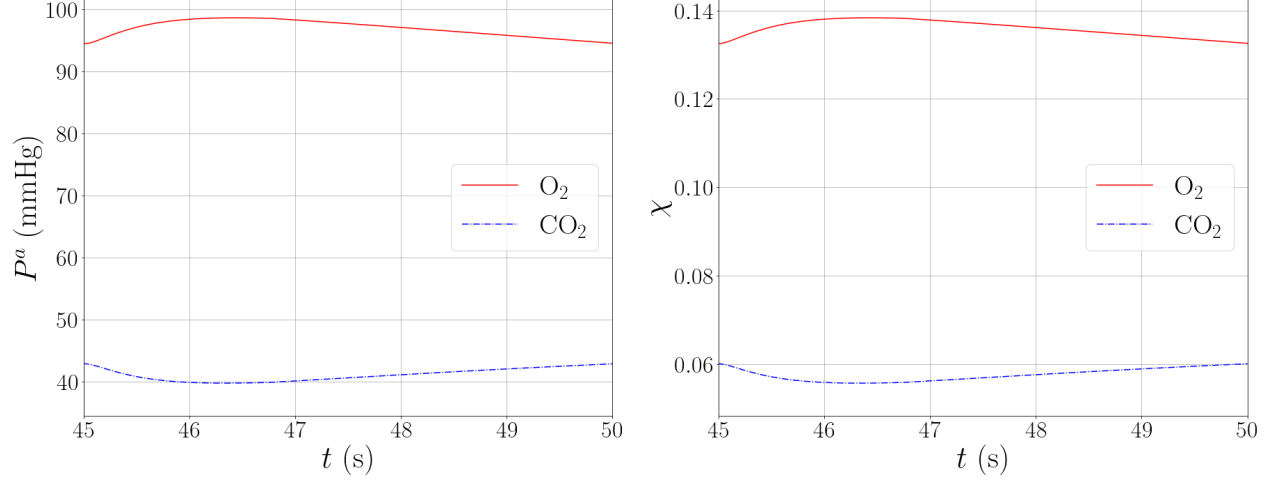


FIGURE 11. Plots w.r.t. time of (a) the arterial (or oxygenated) blood partial pressures $P_{O_2}^a$, $P_{CO_2}^a$, and (b) the alveolar mole fractions χ_{O_2} , χ_{CO_2} .

TABLE 2. Averaged gas quantities in the healthy case with $V_D = 0$.

$\langle q_{O_2} \rangle$ (mL/min)	$\langle q_{CO_2} \rangle$ (mL/min)	RQ	$\langle P_{O_2}^a \rangle$ (mmHg)	$\langle P_{CO_2}^a \rangle$ (mmHg)	$\langle \chi_{O_2} \rangle$	$\langle \chi_{CO_2} \rangle$	V_D (L)	V_{min} (L)	V_{max} (L)
273	-326	1.19	116	36.7	16.3%	5.15%	0	2.50	3.05

TABLE 3. Averaged quantities for a healthy hyperventilating patient.

$\langle q_{O_2} \rangle$ (mL/min)	$\langle q_{CO_2} \rangle$ (mL/min)	RQ	$\langle P_{O_2}^a \rangle$ (mmHg)	$\langle P_{CO_2}^a \rangle$ (mmHg)	$\langle \chi_{O_2} \rangle$	$\langle \chi_{CO_2} \rangle$	V_D (L)	V_{min} (L)	V_{max} (L)
267	-267	1	108	38.7	15.2%	5.42%	0.233	2.58	2.99

4.2. Hyperventilation. We can also consider a hyperventilation scenario for a healthy patient, by choosing $T = 2$ s (instead of 5) and $i_{frac} = 0.5$ (instead of 0.35).

We can then observe changes for carbon dioxide quantities in Table 3, compared to Table 1: the absolute value of the carbon dioxide flux significantly increases, whereas the oxygen one remains quite similar, and $\langle P_{CO_2}^a \rangle$ and $\langle \chi_{CO_2} \rangle$ are not significantly impacted. We also note that V_D in that situation is higher than in the normal breathing. The evolution of the lung volume with respect to time is given in Figure 12.

Remark 9. Compared to the static regime, see Remark 6, in the dynamic one, neglecting the Haldane effect implies a carbon dioxide flux reduction of approximately 6% with our model. It may lead to the observation of two adjunct phenomena: a decrease of the carbon dioxide flux which is exhaled, and a decrease of the arterial carbon dioxide partial pressure (hence an increase between the arterial and venous carbon dioxide partial pressures). It is related to the fact that the Haldane effect indeed allows greater carbon dioxide exchanges for a given difference between arterial/venous partial pressures. Even when decreasing this pressure drop, we observe the persistence of the carbon

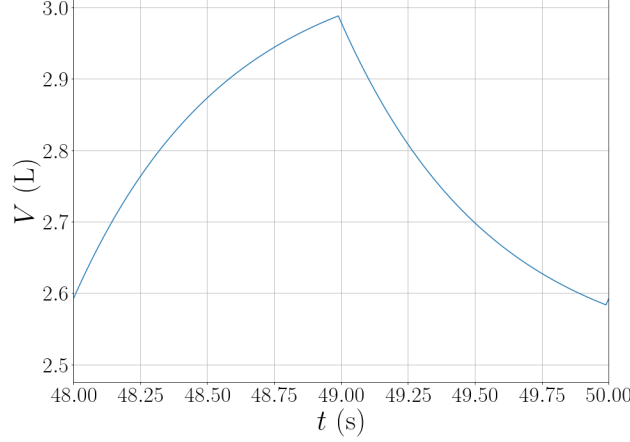


FIGURE 12. Plot w.r.t. time of the total volume V for a healthy hyperventilating patient.

dioxide exchanges, thanks to the influence of oxygen (which binds with hemoglobin, leading to carbon dioxide release).

5. PARAMETER SENSITIVITY

In order to investigate the behaviour of the model in different cases, we lead a sensitivity analysis with respect to the parameters R , E and D_m . Those parameters can take the following values:

$$R = 2^i R^h, \quad -1 \leq i \leq 4, \quad E = 2^j E^h, \quad -4 \leq j \leq 4, \quad D_m = 2^{-k} D_m^h, \quad 0 \leq k \leq 6,$$

remembering that, in any case, we have $D_{m,\text{CO}_2} = 20D_{m,\text{O}_2}$. We choose to focus only on these parameters since they respectively drive the ventilation and diffusion processes.

5.1. Global structuration. To perform this study, 378 numerical simulations of our model were run. For each set of parameters, we plotted coloured dots whose coordinates are either $(\langle q_{\text{O}_2} \rangle, \langle q_{\text{CO}_2} \rangle)$ on Figures 13–15a or $(\langle P_{\text{O}_2}^a \rangle, \langle P_{\text{CO}_2}^a \rangle)$ on Figures 13–15b. The red colour is associated to R , the green one to E and the blue one to D_m .

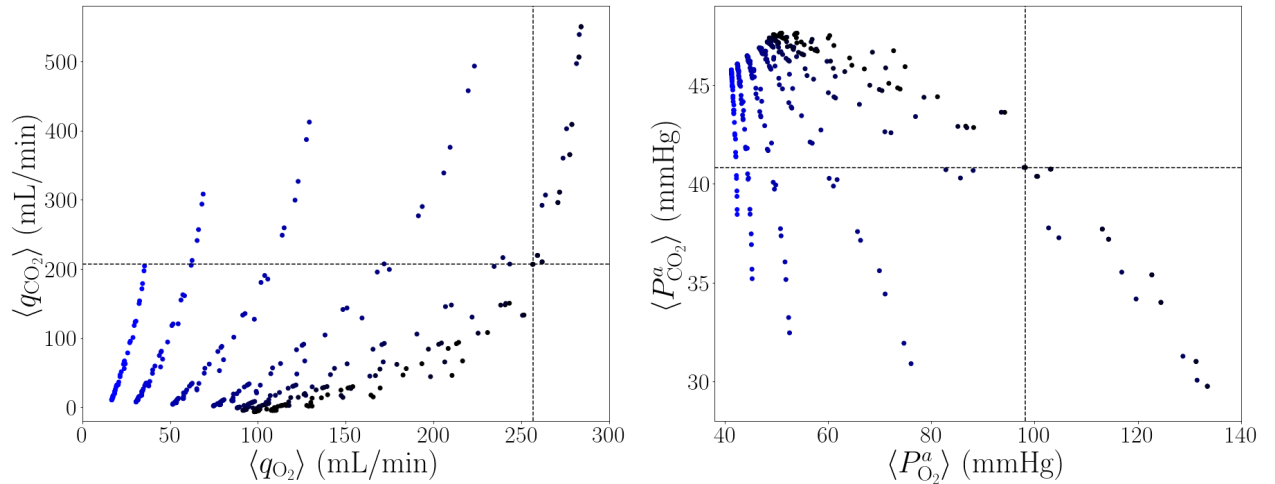


FIGURE 13. Plots with averaged (a) fluxes of O_2 and CO_2 , (b) arterial partial pressures of O_2 and CO_2 , with blue-scaled values of the diffusion coefficients D_m .

In Figure 13, light (respectively dark) blue corresponds to the smaller (respectively higher) values of D_m . On the contrary, in Figure 14, light (respectively dark) green corresponds to the higher (respectively smaller) values of E , and the same goes for Figure 15 with the red colour.

In each figure, the intersection of the two vertical and horizontal lines provides the healthy reference situation defined in Section 4.

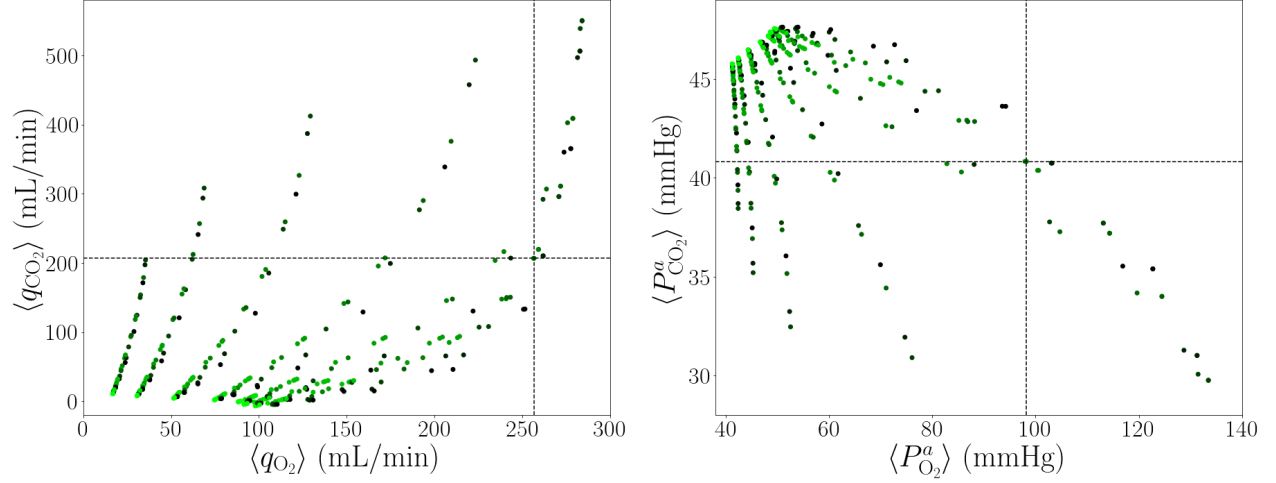


FIGURE 14. Plots with averaged (a) fluxes of O_2 and CO_2 , (b) arterial partial pressures of O_2 and CO_2 , with green-scaled values of E .

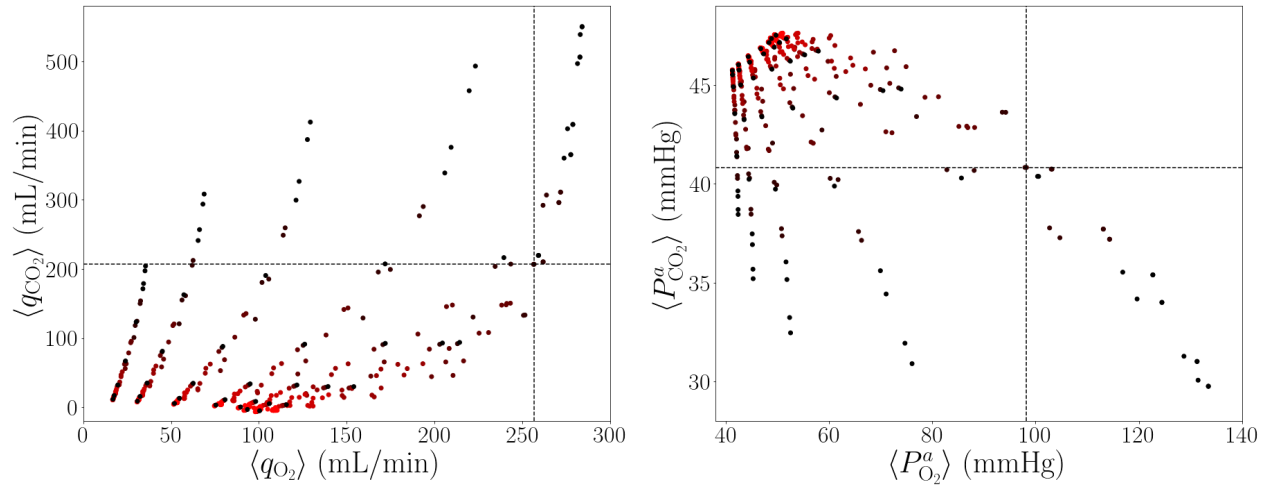


FIGURE 15. Plots with averaged (a) fluxes of O_2 and CO_2 , (b) arterial partial pressures of O_2 and CO_2 , with red-scaled values of R .

In all Figures 13–15, with respect to the healthy reference values, there is a quadrant where there is no plotted dot. It seems hypercapnia and hyperoxia cannot simultaneously happen in our model with the chosen range of parameters. We can observe branched patterns with respect to D_m , see Figure 13, whereas there is no clear structure appearing in Figures 14–15 with respect to E or R .

In Figure 13, the coefficients D_m seem to drive the behaviour of $\langle P_{O_2}^a \rangle$: $\langle P_{O_2}^a \rangle$ decreases when D_m decrease too.

Moreover, the upper left quadrant of Figures 13–15b corresponds to high values of $\langle P_{CO_2}^a \rangle$ and low values of $\langle P_{O_2}^a \rangle$. They can be obtained in several pathological cases: for large E (fibrosis), or normal E and large R (asthma). For small values of E , which can model emphysema, $\langle P_{O_2}^a \rangle$ is larger than in the normal case and $\langle P_{CO_2}^a \rangle$ is lower: dots are in the lower right quadrant. In this situation, when increasing R , the dots are shifted towards the upper left quadrant. Moreover, decreasing D_m first impacts the oxygen transfer, so that dots are shifted to the left (lower left quadrant) before impacting the carbon dioxide transfer. We also checked that there is no particular structure rising with respect to $\tau = R/E$. To further investigate possible patterns, we separate in Figure 16 the cases when $E \leq E^h$ and $E \geq E^h$ for the dots plotted in Figure 15b. More structures with respect to the resistance value R are observed in particular in the emphysema case: $\langle P_{CO_2}^a \rangle$ increases when R increases too, see Figure 16b.

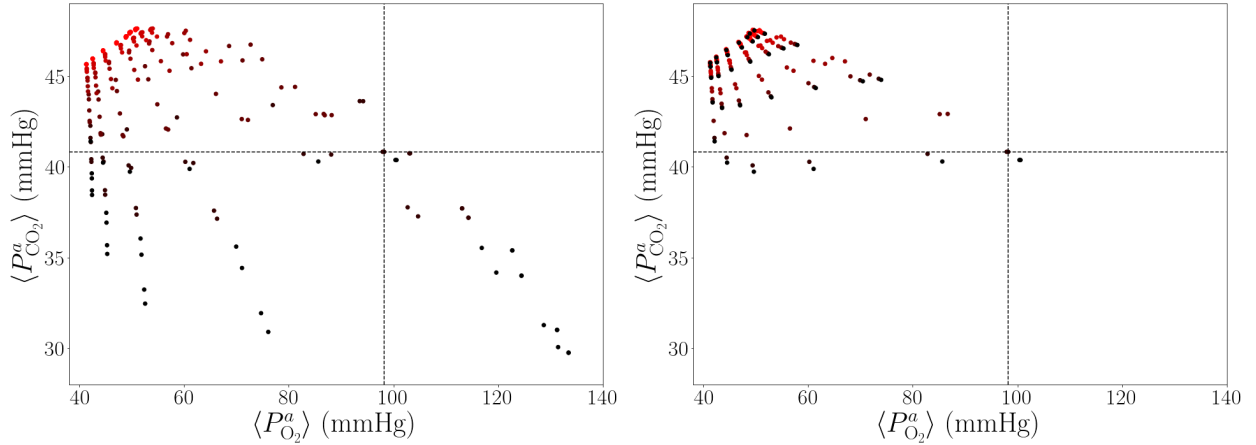


FIGURE 16. Plots with averaged arterial partial pressures of O_2 and CO_2 for (a) $E \leq E^h$ and (b) $E \geq E^h$, with red-scaled values of R .

5.2. Crossed sensitivity structuring. In this subsection, we investigate the crossed sensitivity with respect to the parameters (R, E, D_m) , by setting one of them at its healthy value and letting the two other vary. We choose the oxygen and carbon dioxide arterial partial pressures as outputs. Again, remember that D_{m,CO_2} and D_{m,O_2} are always related by $D_{m,CO_2} = 20D_{m,O_2}$.

Healthy resistance. We first plot $\langle P_{O_2}^a \rangle$ and $\langle P_{CO_2}^a \rangle$ with respect to E , for the considered values of D_m and $R = R^h$ in Figure 17.

When E is close to E^h , there is no variation of $\langle P_{CO_2}^a \rangle$ with respect to D_m , which is not the case for $\langle P_{O_2}^a \rangle$. Note moreover that the variations of $\langle P_{CO_2}^a \rangle$ with respect to D_m for each value of E are small. This is not the case for $\langle P_{O_2}^a \rangle$, which is sensitive to D_m , in particular when E is smaller than E^h . For small degradations of D_m and $E \leq E^h$, we observe moreover a non-monotonic behaviour of $\langle P_{O_2}^a \rangle$ with respect to E : when E decreases, $\langle P_{O_2}^a \rangle$ first increases before decreasing.

Remark 10. *The non-monotonic phenomenon observed in Figure 17 is due to the fact that the model takes into account the increase of the dead space in pathological situations. Indeed, by considering $V_D^P = 0$, we obtain Figure 18.*

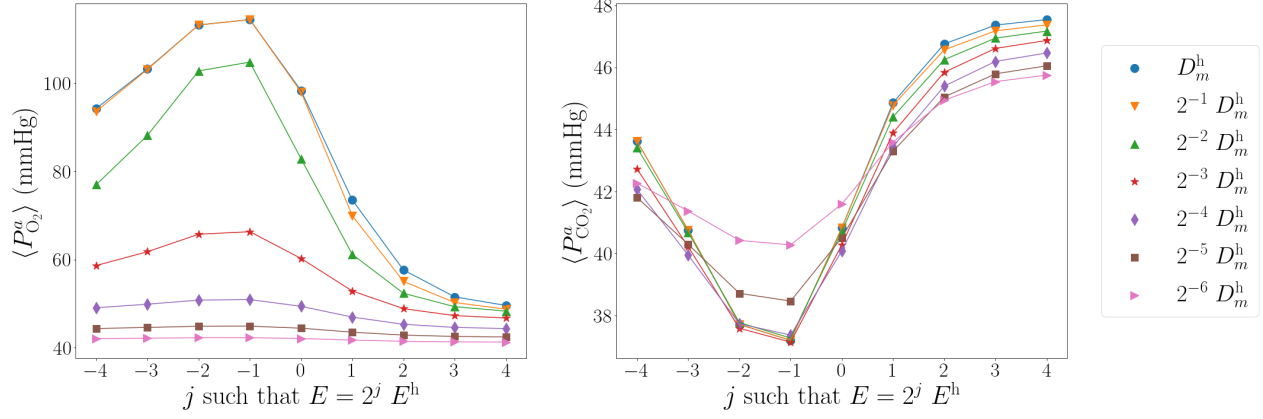


FIGURE 17. Plots of (a) $\langle P_{O_2}^a \rangle$ and (b) $\langle P_{CO_2}^a \rangle$ w.r.t. E , for various diffusion coefficients (with $D_{m,CO_2} = 20D_{m,O_2}$)

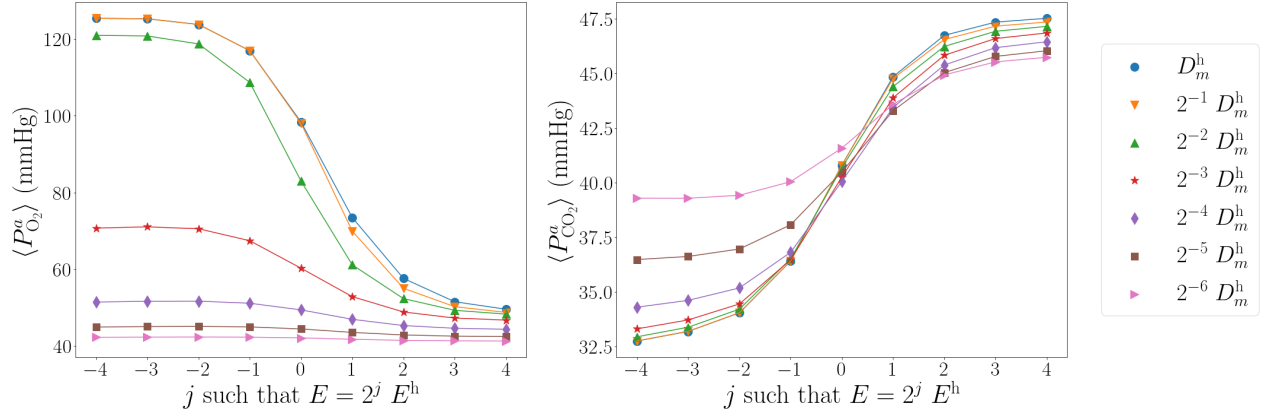


FIGURE 18. Plots of (a) $\langle P_{O_2}^a \rangle$ and (b) $\langle P_{CO_2}^a \rangle$ w.r.t. E , for various diffusion coefficients (with $D_{m,CO_2} = 20D_{m,O_2}$), when choosing $V_D^P = 0$.

Not taking into account the dead space volume increase in emphysema situations implies that the values of arterial partial pressures for low elastances are mostly determined by the values of the diffusivities. In particular, a seemingly non-physiological phenomenon rises: $\langle P_{O_2}^a \rangle$ stays at a really high level, when D_m equals $D_m^h/2$ and $D_m^h/4$, even for degraded elastance.

In Figure 19, $\langle P_{O_2}^a \rangle$ and $\langle P_{CO_2}^a \rangle$ are plotted with respect to the D_m parameters, for the various considered values of E . We emphasize again that we have $D_{m,CO_2} = 20D_{m,O_2}$ in any situation. We can observe that there is no significant effect of D_m on the variation of $\langle P_{CO_2}^a \rangle$, whereas the jump on $\langle P_{O_2}^a \rangle$ is significant between $D_m^h/4$ and $D_m^h/8$, except for higher values of E , for which $\langle P_{O_2}^a \rangle$ is already very low. More precisely, $\langle P_{CO_2}^a \rangle$ remains close to a constant value for each E (excepting larger values of E and degraded values of D_m), so that $\langle P_{CO_2}^a \rangle$ can be seen as a good indicator of lung stiffness. Yet, due to the non-monotonic behaviour with respect to E , the values of $\langle P_{CO_2}^a \rangle$ are nearly the same for $E = E^h$ and $E = E^h/8$.

Healthy diffusion parameters. We now set the D_m coefficients at their healthy values D_m^h . In Figure 20, we consider the variations of $\langle P_{O_2}^a \rangle$ and $\langle P_{CO_2}^a \rangle$ with respect to E , for various R . We observe that, for each value of E , the arterial partial pressures are monotonic with respect to R :

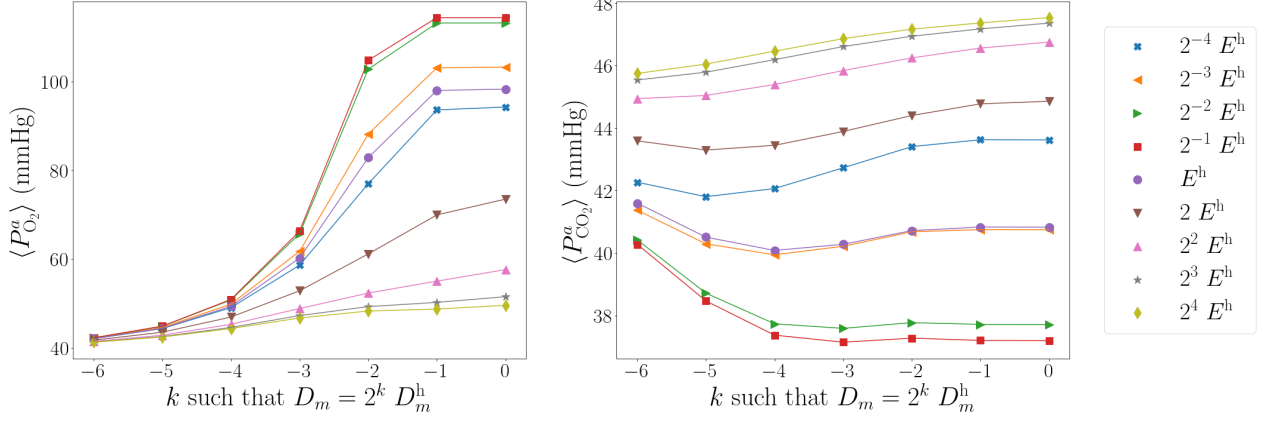


FIGURE 19. Plots of (a) $\langle P_{O_2}^a \rangle$ and (b) $\langle P_{CO_2}^a \rangle$ w.r.t. the D_m parameters, for various E .

$\langle P_{O_2}^a \rangle$ decreases as R increases, whereas $\langle P_{CO_2}^a \rangle$ increases. When E is large there is almost no variation in the partial pressures with respect to R . When E is lower than E^h , the same nonlinear behaviour as before appears, once again due to the increase of the dead space volume.

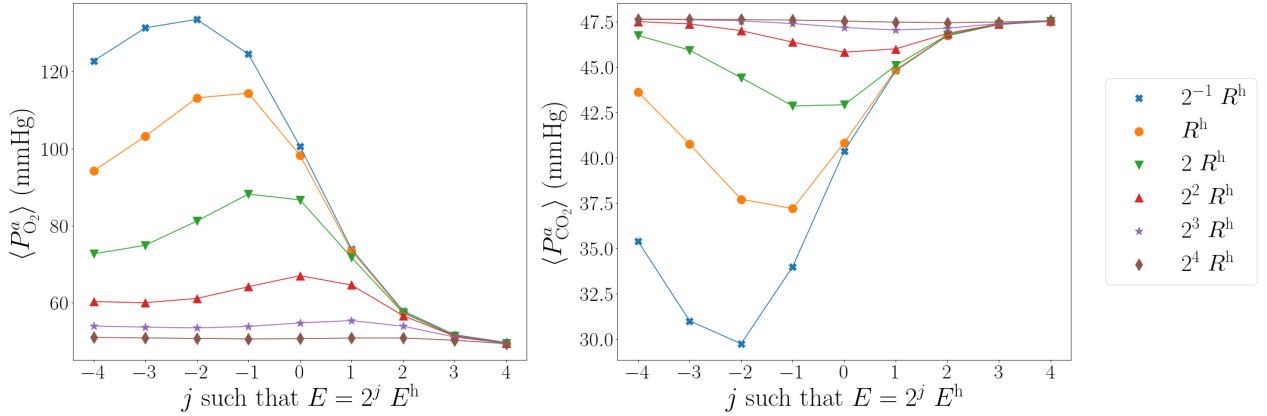
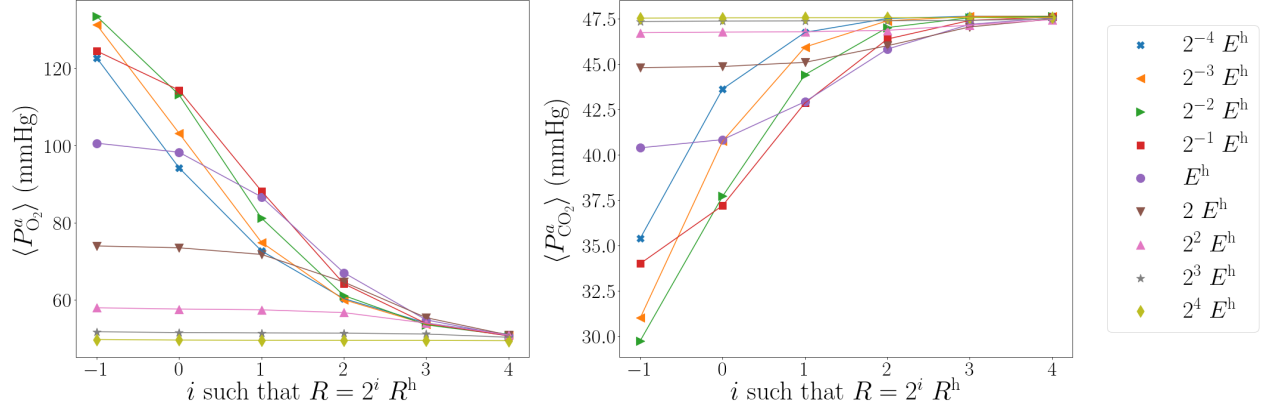
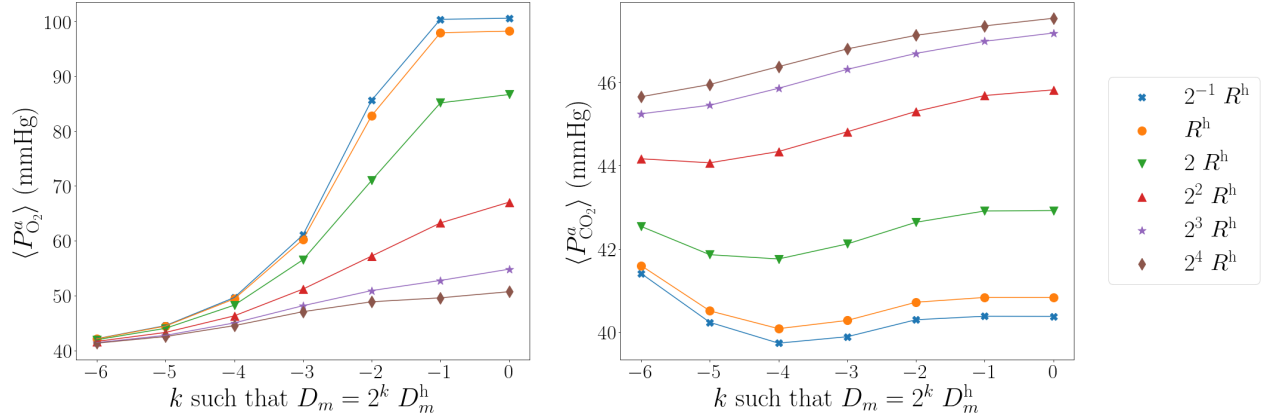


FIGURE 20. Plots of (a) $\langle P_{O_2}^a \rangle$ and (b) $\langle P_{CO_2}^a \rangle$ w.r.t. E , for various R .

In Figure 21, we plot the arterial partial pressures with respect to R . We observe that, for each value of E , they are monotonic in R and they quickly reach a limit value when R increases. There is no monotonicity for a given value of R with respect to E .

Healthy elastance. Finally, we set E at its healthy value E^h , and consider the variations with respect to R and D_m . Figure 22 shows that $\langle P_{O_2}^a \rangle$ and $\langle P_{CO_2}^a \rangle$ are monotonic in R , but not in D_m . Moreover, $\langle P_{O_2}^a \rangle$ is really sensitive to D_m for values of R close the healthy reference value, and $\langle P_{CO_2}^a \rangle$ has almost a constant value for each R .

To conclude, as expected, the oxygen arterial partial pressure is more sensitive to the variations of D_m than the carbon dioxide one. Furthermore, taking into account the dead space volume induces some nonlinear effects and non-monotonic behaviour of the arterial partial pressures. We also observe that highly pathological situations can lead to similar output values, yet the path to

FIGURE 21. Plots of (a) $\langle P_{O_2}^a \rangle$ and (b) $\langle P_{CO_2}^a \rangle$ w.r.t. R , for various E .FIGURE 22. Plots of (a) $\langle P_{O_2}^a \rangle$ and (b) $\langle P_{CO_2}^a \rangle$ w.r.t. the D_m parameters, for various R .

those critical values in the parameter space seems to depend on the considered pathologies. Note, however, that, so far, we have used only one breathing scenario. In the next section, we thus further investigate different pathological situations and the effects of different breathing scenarios.

6. CHARACTERISTIC CASES, TENDENCIES

In this section, we exhibit several pathological situations, by varying one or several parameters, illustrating the model ability to recover known qualitative behaviours.

6.1. Happy hypoxia. Degrading the D_m parameters, while always keeping $D_{m,CO_2} = 20 D_{m,O_2}$, translates damaging of the membrane where the gaseous exchanges happen. This deterioration numerically induces, in our model, a so-called happy hypoxia effect. Indeed, as we can see in Tables 4–5, compared to Table 1, the oxygen flux drastically drops, and more oxygen is stored in the lung, since the membrane is damaged. The effect on carbon dioxide exchanges is not as significant.

6.2. Asthma. Asthma can be roughly modelled by increasing the resistance of the bronchial tree, since, in particular, it is characterized by some bronchi constriction. In Tables 6–7, we observe that the carbon dioxide flux drastically goes down, whereas the effect on the oxygen flux appears as less

TABLE 4. Averaged quantities with $D_m = D_m^h/4$.

$\langle q_{O_2} \rangle$ (mL/min)	$\langle q_{CO_2} \rangle$ (mL/min)	RQ	$\langle P_{O_2}^a \rangle$ (mmHg)	$\langle P_{CO_2}^a \rangle$ (mmHg)	$\langle \chi_{O_2} \rangle$ –	$\langle \chi_{CO_2} \rangle$ –	V_D (L)	V_{\min} (L)	V_{\max} (L)
233	–200	0.858	82.1	40.8	14.2%	5.65%	0.152	2.50	3.05

TABLE 5. Averaged quantities with $D_m = D_m^h/8$.

$\langle q_{O_2} \rangle$ (mL/min)	$\langle q_{CO_2} \rangle$ (mL/min)	RQ	$\langle P_{O_2}^a \rangle$ (mmHg)	$\langle P_{CO_2}^a \rangle$ (mmHg)	$\langle \chi_{O_2} \rangle$ –	$\langle \chi_{CO_2} \rangle$ –	V_D (L)	V_{\min} (L)	V_{\max} (L)
167	–192	1.15	60	40.4	15.5%	5.43%	0.152	2.50	3.05

significant. Besides, the carbon dioxide exchanges are lowered, leading to rising CO_2 concentrations in both the lung and the blood, and consequently to acidosis ($P_{CO_2}^a \geq 45$ mmHg). Moreover, we clearly see the decreasing of the total volume amplitude over a breathing period with respect to a healthy patient and thus the increase of the dead space volume.

TABLE 6. Averaged quantities with $R = 2R^h$.

$\langle q_{O_2} \rangle$ (mL/min)	$\langle q_{CO_2} \rangle$ (mL/min)	RQ	$\langle P_{O_2}^a \rangle$ (mmHg)	$\langle P_{CO_2}^a \rangle$ (mmHg)	$\langle \chi_{O_2} \rangle$ –	$\langle \chi_{CO_2} \rangle$ –	V_D (L)	V_{\min} (L)	V_{\max} (L)
240	–146.	0.607	86.2	43	12.1%	6.03%	0.176	2.53	2.96

TABLE 7. Averaged quantities with $R = 4R^h$.

$\langle q_{O_2} \rangle$ (mL/min)	$\langle q_{CO_2} \rangle$ (mL/min)	RQ	$\langle P_{O_2}^a \rangle$ (mmHg)	$\langle P_{CO_2}^a \rangle$ (mmHg)	$\langle \chi_{O_2} \rangle$ –	$\langle \chi_{CO_2} \rangle$ –	V_D (L)	V_{\min} (L)	V_{\max} (L)
193	–62.2	0.323	66.9	45.8	9.42%	6.43%	0.234	2.58	2.85

For strong asthma ($R = 4R^h$ in the cases we study below), the patient can try to adapt his respiration to balance the asthma effect. We investigate two different scenarios.

In the first one, the breathing period is reduced at $T = 2$ s, and the inspiration proportion is increased at $i_{\text{frac}} = 0.5$: we consider again a hyperventilating patient as in Table 3. Table 8 confirms that hyperventilation is not at all a proper response to asthma.

In the second one, we trigger an active expiration, *i.e.* we involve a positive pressure at expiration, namely $P_{\text{ext}}(t) = 2.00$ when $i_{\text{frac}}T \leq t < T$, with $i_{\text{frac}} = 0.35$ and $T = 5$ s again. The respiration improvement is then observed in Table 9, where we recover values very close to the healthy ones in Table 1, in particular because the dead space volume becomes again equal to the anatomical one because of the active expiration process.

TABLE 8. Averaged quantities with $R = 4R^h$ and hyperventilation.

$\langle q_{O_2} \rangle$ (mL/min)	$\langle q_{CO_2} \rangle$ (mL/min)	RQ	$\langle P_{O_2}^a \rangle$ (mmHg)	$\langle P_{CO_2}^a \rangle$ (mmHg)	$\langle \chi_{O_2} \rangle$ –	$\langle \chi_{CO_2} \rangle$ –	V_D (L)	V_{\min} (L)	V_{\max} (L)
151	–26.6	0.176	57.3	46.8	8.16%	6.56%	0.374	2.72	2.85

TABLE 9. Averaged quantities with $R = 4R^h$ and active expiration.

$\langle q_{O_2} \rangle$ (mL/min)	$\langle q_{CO_2} \rangle$ (mL/min)	RQ	$\langle P_{O_2}^a \rangle$ (mmHg)	$\langle P_{CO_2}^a \rangle$ (mmHg)	$\langle \chi_{O_2} \rangle$ –	$\langle \chi_{CO_2} \rangle$ –	V_D (L)	V_{\min} (L)	V_{\max} (L)
254	–199	0.783	95.8	41.1	13.4%	5.76%	0.150	2.10	2.62

6.3. Pathologies affecting tissue elasticity.

6.3.1. *Fibrosis.* Increasing elastance E is characteristic of lung fibrosis. In both Tables 10–11, E is chosen as $E = 2E^h$, whereas the D_m parameters are set to their healthy values in Table 10, and to $D_m^h/4$ in Table 11. Indeed, the tissue damage can also have an effect on the diffusivities. The lung volume remains the same in both situations.

TABLE 10. Averaged quantities with $E = 2E^h$.

$\langle q_{O_2} \rangle$ (mL/min)	$\langle q_{CO_2} \rangle$ (mL/min)	RQ	$\langle P_{O_2}^a \rangle$ (mmHg)	$\langle P_{CO_2}^a \rangle$ (mmHg)	$\langle \chi_{O_2} \rangle$ –	$\langle \chi_{CO_2} \rangle$ –	V_D (L)	V_{\min} (L)	V_{\max} (L)
211	–88.5	0.420	72.7	45.0	10.2%	6.31%	0.150	2.50	2.79

TABLE 11. Averaged quantities with $E = 2E^h$ and $D_m = D_m^h/4$.

$\langle q_{O_2} \rangle$ (mL/min)	$\langle q_{CO_2} \rangle$ (mL/min)	RQ	$\langle P_{O_2}^a \rangle$ (mmHg)	$\langle P_{CO_2}^a \rangle$ (mmHg)	$\langle \chi_{O_2} \rangle$ –	$\langle \chi_{CO_2} \rangle$ –	V_D (L)	V_{\min} (L)	V_{\max} (L)
168	–87.3	0.519	60.6	44.5	11.3%	6.19%	0.150	2.50	2.79

In any case, the elastance increasing leads to drastically low values of carbon dioxide flux, whereas the diffusivity decreasing reduces the oxygen flux. Consequently, in the acini and in the blood, the concentration and partial pressure of carbon dioxide are too high, and the oxygen one is far too low.

6.3.2. *Emphysema.* When we model emphysema and the subsequent tissue deterioration through elastance decreasing only, we obtain the results from Table 12 for $E = E^h/4$.

TABLE 12. Averaged quantities with $E = E^h/4$.

$\langle q_{O_2} \rangle$ (mL/min)	$\langle q_{CO_2} \rangle$ (mL/min)	RQ	$\langle P_{O_2}^a \rangle$ (mmHg)	$\langle P_{CO_2}^a \rangle$ (mmHg)	$\langle \chi_{O_2} \rangle$ –	$\langle \chi_{CO_2} \rangle$ –	V_D (L)	V_{\min} (L)	V_{\max} (L)
271	–293	1.08	113	37.8	0.158	0.0530	0.484	2.83	3.88

Emphysema destroys the alveolar tissues and leads to air trapping, implying increasing the dead space volume. Adding a degradation of D_m as $D_m = D_m^h/4$, we obtain the results presented in Table 13, where the values are close to normal ones, confirming that emphysema can be really tricky to detect.

TABLE 13. Averaged quantities with $E = E^h/4$, and $D_m = D_m^h/4$.

$\langle q_{O_2} \rangle$ (mL/min)	$\langle q_{CO_2} \rangle$ (mL/min)	RQ	$\langle P_{O_2}^a \rangle$ (mmHg)	$\langle P_{CO_2}^a \rangle$ (mmHg)	$\langle \chi_{O_2} \rangle$ –	$\langle \chi_{CO_2} \rangle$ –	V_D (L)	V_{\min} (L)	V_{\max} (L)
261	–289	1.11	102	37.9	16.0%	5.23%	0.484	2.83	3.88

Next, further degrading the diffusion coefficients with $D_m = D_m^h/8$ and still considering $E = E^h/4$, we get the results from Table 14. We see there a serious drop of the oxygen partial pressure whereas the carbon dioxide partial pressure is still low. To be able to have an impact on the carbon dioxide partial pressure, one may increase the resistance and consider for instance $R = 4R^h$. In this case, in Table 15, the effects become very clear, in the same way as in the asthma case, leading to respiratory acidosis.

TABLE 14. Averaged quantities with $E = E^h/4$, and $D_m = D_m^h/8$.

$\langle q_{O_2} \rangle$ (mL/min)	$\langle q_{CO_2} \rangle$ (mL/min)	RQ	$\langle P_{O_2}^a \rangle$ (mmHg)	$\langle P_{CO_2}^a \rangle$ (mmHg)	$\langle \chi_{O_2} \rangle$ –	$\langle \chi_{CO_2} \rangle$ –	V_D (L)	V_{\min} (L)	V_{\max} (L)
191	–274	1.44	65.6	37.7	17.1%	4.96%	0.484	2.83	3.88

TABLE 15. Averaged quantities with $E = E^h/4$, $D_{m,O_2} = D_{m,O_2}^h/4$ and $R = 4R^h$.

$\langle q_{O_2} \rangle$ (mL/min)	$\langle q_{CO_2} \rangle$ (mL/min)	RQ	$\langle P_{O_2}^a \rangle$ (mmHg)	$\langle P_{CO_2}^a \rangle$ (mmHg)	$\langle \chi_{O_2} \rangle$ –	$\langle \chi_{CO_2} \rangle$ –	V_D (L)	V_{\min} (L)	V_{\max} (L)
131	–291	0.223	53.9	46.4	9.96%	6.47%	0.814	3.16	3.45

Remark 11. Note that, if the modification of the dead space volume is not taken into account (namely, by setting $V_D^P = 0$), we obtain non-physiological results with a too high carbon dioxide flux.

7. CONCLUSION

We propose a nonlinear coupled dynamical model of ventilation-perfusion for oxygen and carbon dioxide, taking into account the Bohr and Haldane effects. The model is based upon conservation laws (mechanics and gas exchange) and phenomenological ones (gas interaction). It is only driven by the action of the respiration muscles. Moreover we introduce a new definition of the dead space depending on the patient state and the breathing scenarios. We quantitatively recover acknowledged observable values for a healthy patient, and exhibit realistic qualitative behaviours in pathological situations. We observe that the Haldane effect is crucial to capture the expected orders of magnitude for gas transfer, even if this effect is lowered in the dynamical regime, see Remarks 6 and 9. It is also the case for the pathological dead space, see Remarks 8, 10 and 11. The sensitivity analysis represents a first step towards classification of the pathological behaviours with respect to the considered input parameters. Yet we also point out that similar output values can be reached from very different sets of input parameters. Those outputs may not allow to discriminate straightforwardly between patients or pathologies. However, since the patient final state results from various successive parameter degradations, our model may help to understand the patient history. Alternatively, it can be used to define other relevant biomarkers as well as breathing scenarios to classify pathological states or histories.

This ventilation-gas diffusion model, accounting for both Bohr and Haldane effects, may further be used as a part of more complex ODE or PDE systems, for instance by coupling it to cardiovascular models (through the connection to parameters such as the transit time of a red blood cell in the acinar region τ_b and the capillary volume V_c), or by considering it in a one-dimensional transport-diffusion model of air in the airways. In this case, it would generalize previous works, which only considered oxygen in [19] or without coupling between the two species in [22, 23]. In particular, it is crucial to take into account the transport phenomena to accurately describe the delay that occurs in the gas exchanges, allowing for instance optimisation strategies for breathing scenarios.

APPENDIX A. PARAMETERS

We consider the following set of parameters corresponding to the standard situation of a healthy person at rest, see Table 16.

REFERENCES

- [1] G. S. Adair. The hemoglobin system. VI. The oxygen dissociation curve of hemoglobin, *J. Biol. Chem.*, 63:529–545 (1925).
- [2] L. Baffico, C. Grandmont and B. Maury. Multiscale modeling of the respiratory tract, *Math. Models Methods Appl. Sci.* 20(1): 59–93 (2010).
- [3] J. H. T. Bates. *Lung mechanics, an inverse modeling approach*, Cambridge University Press (2009). *The Respiratory System in Equations*, Springer, MS&A (2013).
- [4] R. Begin, A. D. Renzetti Jr., A. H. Bigler and S. Watanabe. Flow and age dependence of airway closure and dynamic compliance, *J. Appl. Physiol.*, 38(2):199–207 (1975).
- [5] A. Ben-Tal. Simplified models for gas exchange in the human lungs, *J. Theor. Biol.*, 238:474–495 (2006).
- [6] L. Berger, R. Bordas, K. Burrowes, V. Grau, S. Tavener and D. Kay. A poroelastic model coupled to a fluid network with applications in lung modelling, *Int. J. Numer. Meth. Biomed. Engng.* 32(1):e02731 (2015).
- [7] C. Brighenti, G. Gnudi and G. Avanzolini. A simulation model of the oxygen alveolo-capillary exchange in normal and pathological conditions, *Physiol. Meas.*, 24:261–275 (2003).
- [8] L. Cheng, O. Ivanova, H. H. Fan and M. C. K. Khoo. An integrative model of respiratory and cardiovascular control in sleep-disordered breathing. *Respir. Physiol. Neurobiol.* 174:4–28 (2010).
- [9] B. J. B. Grant. Influence of Bohr-Haldane effect on steady-state gas exchange, *J. Appl. Physiol. Respir. Environ. Exerc. Physiol.*, 52:1330–1337 (1982).
- [10] A. C. Guyton and J. E. Hall. *Textbook of Medical Physiology*, 9th ed., W.B. Saunders Co, Philadelphia (1996).
- [11] E. P. Hill, G. G. Power and L. D. Longo. Kinetics of O₂ and CO₂ exchange. In: *Bioengineering aspects of the lung*, 459–514, Dekker, New York, USA (1977).
- [12] M. P. Hlastala and A. J. Berger. *Physiology of Respiration*, 2nd ed. Oxford University Press (2001).

TABLE 16. Standard values of some physiological parameters.

Mechanical parameters			Ref.
Elastance	E	3.5 cmH ₂ O · L ⁻¹	[10, 4, 5]
Resistance	R	2 cmH ₂ O · s · L ⁻¹	[10, 5]
Functional residual capacity	FRC	3 L	[10, 29, 16]
Anatomical dead space	V_D^A	0.15 L	[34]
Gas exchange parameters			Ref.
Reduced atmospheric pressure	P_{atm}	713 mmHg	[10, 5]
Mole fraction in fresh air for O ₂	$\chi_{\text{O}_2}^{\text{atm}}$	21% –	[10]
Mole fraction in fresh air for CO ₂	$\chi_{\text{CO}_2}^{\text{atm}}$	0.04% –	[10]
Membrane diffusing capacity (O ₂)	D_{m,O_2}	21 mL · min ⁻¹ · mmHg ⁻¹	[10, 5]
Membrane diffusing capacity (CO ₂)	D_{m,CO_2}	420 mL · min ⁻¹ · mmHg ⁻¹	[10]
Capillary volume	V_c	70 mL	[5, 10, 34]
Transit time of red blood cells in V_c	τ_b	0.75 s	[34, 14, 5]
Pressure of O ₂ in venous blood	$P_{\text{O}_2}^v$	40 mmHg	[34, 10]
Pressure of CO ₂ in venous blood	$P_{\text{CO}_2}^v$	46 mmHg	[34, 10]
Concentration of hemoglobin	C_{Hb}	$2.2 \cdot 10^{-3}$ mol · L ⁻¹	[12, 5]
Solubility of O ₂ in plasma	σ	$1.4 \cdot 10^{-6}$ mol · L ⁻¹ · mmHg ⁻¹	[14, 5]
Acidity	pH	7.4 –	[34, 10]
Dissociation const. of carbonic acid	pK_A	6.1 –	[34]
Concentration of bicarbonate	$C_{\text{HCO}_3^-}$	$24 \cdot 10^{-3}$ mol · L ⁻¹	[34]
Observable quantities			Ref.
Tidal volume [max $V(t)$ – FRC]	V_T	0.50 L	[34, 29]
Air flow	\dot{V}	± 0.50 L · s ⁻¹	[34]
Mean alveolar pressure of O ₂	$\langle P_{\text{O}_2}^a \rangle$	100 mmHg	[34, 10, 5, 16]
Mean alveolar pressure of CO ₂	$\langle P_{\text{CO}_2}^a \rangle$	40 mmHg	[34, 10]
Mean alveolar mole fraction of O ₂	$\langle \chi_{\text{O}_2} \rangle$	15% –	[34, 10, 5, 16]
Mean alveolar mole fraction of CO ₂	$\langle \chi_{\text{CO}_2} \rangle$	4% –	[34, 10]
Mean O ₂ transfer rate	q_{O_2}	0.25 L · min ⁻¹	[34, 10, 33]
Mean CO ₂ transfer rate	q_{CO_2}	0.20 L · min ⁻¹	[34, 10]
Respiratory quotient	RQ	0.8 –	[34, 10]

- [13] M. Ismail, A. Comerford and W. A. Wall. Coupled and reduced dimensional modeling of respiratory mechanics during spontaneous breathing, *Int. J. Numer. Meth. Biomed. Engng.* 29:1285–1305 (2013).
- [14] J. Keener and J. Sneyd. *Mathematical Physiology*, Interdisciplinary Applied Mathematics, Springer (1998).
- [15] G. R. Kelman. Digital computer subroutine for the conversion of oxygen tension into saturation, *J. Appl. Physiol.*, 21(4):1375–1376 (1966).
- [16] J. D. Kibble and C. Halsey. *Medical Physiology, The Big Picture*, McGraw Hill (2009).
- [17] J. A. Loeppky, U. C. Luft and E. R. Fletcher. Quantitative description of whole blood CO₂ dissociation curve and Haldane effect, *Respir. Physiol.*, 51:167–181 (1983).
- [18] H. Malte and G. Lykkeboe. The Bohr/Haldane effect: a model-based uncovering of the full extent of its impact on O₂ delivery to and CO₂ removal from tissues, *J. Appl. Physiol.*, 125:916–922 (2018).
- [19] S. Martin and B. Maury. Modeling of the oxygen transfer in the respiratory process, *ESAIM Math. Model. Numer. Anal.*, 47(4):935–960 (2013).
- [20] B. Maury. *The Respiratory System in Equations*, Springer, MS&A (2013).
- [21] F. Meade. A formula for the carbon dioxide dissociation curve, *Br. J. Anaesth.*, 44(6):630 (1972).

- [22] F. Noël and B. Mauroy. Interplay between optimal ventilation and gas transport in a model of the human lung, *Front. Physiol.*, 10:488 (2019).
- [23] F. Noël, C. Karamaoun, J. Dempsey and B. Mauroy. The origin of the allometric scaling of lung ventilation in mammals, *arXiv, 2005.12362, ver. 6, peer-reviewed and recommended by Peer community in Mathematical and Computational Biology* (2021).
- [24] J. M. Oakes, A. L. Marsden, C. Grandmont, S. C. Shadden, C. Darquenne and I. Vignon-Clémentel. Airflow and particle deposition simulations in health and emphysema: from in vivo to in silico animal experiments, *Ann. Biomed. Engng.*, 42(4):899–914, 2014.
- [25] N. Pozin, S. Montesantos, I. Katz, M. Pichelin, I. Vignon-Clémentel and C. Grandmont. A tree-parenchyma coupled model for lung ventilation simulation. *Int. J. Numer. Meth. Biomed. Engng.* 33:e2873 (2017).
- [26] C. J. Roth, M. Ismail, L. Yoshihara and W. A. Wall. A comprehensive computational human lung model incorporating inter-acinar dependencies: application to spontaneous breathing and mechanical ventilation, *Int. J. Numer. Meth. Biomed. Engng.* 33(1):e02787 (2015).
- [27] T. Similowski and J. H. T. Bates. Two-compartment modelling of respiratory system mechanics at low frequencies: gas redistribution or tissue rheology?, *Eur. Respir. J.*, 4:353–358 (1991).
- [28] J. L. Spencer, E. Firouztale, and R. B. Mellins. Computational expressions for blood oxygen and carbon dioxide concentrations, *Ann. Biomed. Engng.*, 7:59–66 (1979).
- [29] J. Sznitman. Convective gas transport in the pulmonary acinus: comparing roles of convective and diffusive lengths, *J. Biomech.*, 42:789–792 (2009).
- [30] A. J. Swan, A. R. Clark and M. H. Tawhai. A computational model of the topographic distribution of ventilation in healthy human lungs, *J. Theor. Biol.* 300:222–231 (2012).
- [31] A. J. Swan and M. H. Tawhai. Evidence for minimal oxygen heterogeneity in the healthy human pulmonary acinus, *J. Appl. Physiol.*, 110(2):528–537 (2011).
- [32] E. R. Weibel, *The pathway for oxygen*, Harvard University Press (1984).
- [33] E. R. Weibel, B. Sapoval and M. Filoche. Design of peripheral airways for efficient gas exchange, *Resp. Phys. Neur.*, 148:3–21 (2005).
- [34] J. B. West. *Respiratory Physiology: The Essentials*, Williams & Wilkins (1974).

DECLARATION OF INTERESTS

The authors state that there are no interest to declare.

L.B.: SORBONNE UNIVERSITÉ, CNRS, UNIVERSITÉ PARIS CITÉ, LABORATOIRE JACQUES-LOUIS LIONS (LJLL), F-75005 PARIS, FRANCE

Email address: laurent.boudin@sorbonne-universite.fr

C.G.: INRIA, SORBONNE UNIVERSITÉ, UNIVERSITÉ PARIS CITÉ, CNRS, LABORATOIRE JACQUES-LOUIS LIONS (LJLL), F-75012 PARIS, FRANCE

Email address: celine.grandmont@inria.fr

B.G., S.M.: MAP5, CNRS UMR 8145, UNIVERSITÉ PARIS CITÉ, F-75006 PARIS, FRANCE

Email address: berenice.grec@u-paris.fr, sebastien.martin@u-paris.fr